Changes in mineralogy and porosity during the reaction of shales with fracking fluid, CO_2-fluid and brine

MASTER THESIS

Utrecht University
Department of Earth Sciences
Earth, Structure, and Dynamics

August, 2015

by
Pien Dohmen,
3473627

1st supervisor
dr. Helen E. King

2nd supervisors
dr. Oliver Plümper & dr. Paul R.D. Mason

TABLE OF CONTENTS

ABSTRACT

Shale gas is an unconventional geo-resource, which had lots of attention in the last decade. This is mostly negative attention about the dangers of the chemicals in industrial fracking fluid and its impact on the environment. The methane emissions into the atmosphere are also a large concern when producing shale gas, as it is much higher than those of conventional resources. The challenge of today is to combine the continued use of fossil fuels, while simultaneously also reducing the associated CO_2 emissions. In this study four different type of samples were put under the microscope (using the tabletop-SEM and FIB-SEM). These four samples were all Gothic shales: unreacted Gothic shale; Gothic shale reacted with industrial fracking fluid; Gothic shale reacted with CO_2-fluid; and Gothic shale reacted with brine. The samples investigated in this study were already produced and provided by the group of Dr. Kaszuba at the University of Wyoming who are currently conducting experiments on samples from a US based shale gas site. The aim was to observe the changes in porosity and mineralogy of each sample at the nanoscale and to find out if CO_2-fluid would be a suitable substitute for industrial fracking fluid, while at the same time also reducing the CO_2 emissions into the atmosphere. The unreacted Gothic shale and brine reacted sample showed the least amount of pores. The Gothic shale reacted with CO_2-fluid had larger pores in comparison to the Gothic shale reacted with fracking fluid. This was evident in the larger amount and size of cracks found in the CO_2-fluid samples, but also in a larger increase in pore surface area compared to the fracking fluid samples. At a magnification of 600x the CO_2-fluid contained a total pore surface area of 1581.4 μm^2, in comparison with 1252 μm^2 of the fracking fluid sample (see table 2). The total pore surface area of three different magnifications added up shows that the CO_2-fluid has a total pore surface area of 3831.35 μm^2, compared to a total pore surface of 3722.71 μm^2. This study demonstrates that CO_2-fluid could therefore be suitable as fracking fluid at the nanoscale, as it generates an increase in porosity in the Gothic shale rock, while at the same time it is a more environment-friendly way of producing shale gas as it reduces CO_2-emissions. The reduction of CO_2-emissions can take place in two different ways by injecting CO_2-fluid into a shale gas site. The CO_2 can either react with the shale, forming carbonates, or it reacts with the clays present in the shale, causing the clays to swell. The carbonates are formed when the CO_2-molecules dissociates into different components and reacts with the host rock. The swelling of clays due to CO_2-fluid causes the shale to increase its sealing capacity, resulting in no leakage to the Earth's surface. Both ways of CO_2-reduction due to injection into the subsurface, causes CO_2 to remain in the ground. Unfortunately each shale is different in mineralogy and content, resulting in different reactions with the fluid used. This means that while CO_2-fluid reacts well with the Gothic shale used in this study, it could react differently with another type of shale, clogging up the pores and resulting in a decrease in porosity. The difference in clay content forms the biggest problem for the clogging of the pores, as clays can be non-swelling or swelling clays (forming an increase or decrease in porosity, respectively). Therefore each shale must be investigated separately, before introducing CO_2-fluid as a new and more environmental-friendly fracking fluid.

1. **INTRODUCTION**

Geologists have known for a long time that methane is present in large amounts in subterranean shale rock layers *(Boersma and Johnson, 2012)*. Evidence suggests that over the past century large amounts of methane, coming from shale rock formations, have migrated upwards to other pools of petroleum to be exploited as conventional gas instead of staying in the shale layers as unconventional gas. The difference between conventional and unconventional oil and gas, is that conventional resources are relatively easily exploited, while unconventional resources requires stimulation before production can begin, or it needs stimulation to maintain production *(Stephenson, Valle and Riera-Palou, 2011)*. This results in lower production costs and automatically in higher profit for the oil and gas industry when exploiting conventional resources. Compared to conventional resources, it is presently deemed uneconomical to extract unconventional resources when conventional resources are still producing. But as conventional oil and gas reserves have been decreasing over the past decade and are therefore harder to find and exploit, new methods of recovering oil and gas from unconventional reservoirs are necessary.

1.1 Shale gas

Unconventional resources have low permeability and porosity. This feature makes production from these reservoirs more difficult compared to conventional reservoirs, as additional measures are needed to extract the resources. Production of unconventional hydrocarbons therefore lead to relatively higher production costs, but also lower production rates. Nevertheless this is not a reason for the industry to stop producing resources, because in an era of rising prices for crude oil and natural gas, the ability to produce oil and gas from unconventional reservoirs has become very important *(Lewis and Hughes, 2008)*, but also possible due to the innovation of technology. These improvements in the technology makes it "easier" to extract unconventional resources nowadays. However, unconventional resources still require a lot more effort than extracting conventional resources, and are associated with added environmental risks.

One of the most well-known and discussed unconventional resources, in industry as well as the public media, is shale gas. In the case of shale gas, natural gas is tightly compressed in the tiny seams within dense layers of the shale rock itself *(Boersma and Johnson, 2012)*, but it also contains molecules of natural gas on the surface of the rock grains, which is referred to as

adsorbed gas *(Lewis and Hughes, 2008)*. In the last few years shale gas has become increasingly important for the oil and gas industry. Shale gas reached the news in Europe the last few years, due to the Shale Gas Boom that took over the United States a decade ago *(Barteau and Kota, 2014)*.

1.2 Fracking and its problems

1.2.1 Permeability

To increase the productivity of shale gas the oil and gas industry employs hydraulic fracturing (fracking) to increase the permeability and porosity of the shale. Fracking is a measure that combines innovations in deep well drilling along with horizontal drilling and injecting a large amount of fluid at high pressure (480–850 bar), which in turn fractures the shale along the horizontal plane. The fluid injected at high pressure mainly consists of water and sand (~98%) with various chemicals (flow improvers to keep the sand in suspension, friction reducers, surfactants, corrosion inhibitors, acids, etc.) *(Boersma and Johnson, 2012; Mohajan, 2012; Howarth, Ingraffea and Engelder, 2011)*. The sand and chemicals in the fluid are necessary to keep the fractures open after pumping has stopped.

After the process of fracking has stopped a proportion of the fracking fluid injected rises back to the surface and is collected in the wellhead. The fluid that returns back to the surface when the fracking process is completed can be seperated into two different categories. The first category is the initial water recovered before production starts, which is defined as flowback water (or just flowback) and the second category is the long-term water that returns to the surface while the gas production is taking place, defined as produced water *(Ferrer and Thurman, 2015; Vidic et al., 2013)*. The amount of the flowback water differs in scientific reports; Nicot and Duncan (2012) state that flowback volume represents a few percent to 50%, and Vidic et al. (2013) agrees with this, finding a percentage that lies between 9–53%. In contrast, U.S. Environmental Protection Agency (2012) and Broderick et al. (2011) find that the percentage of flowback volume is a bit higher than the previous statement, with percentages of 15–80%. Vos (2014) and Stephenson, Valle and Riera-Palou (2011) gave even higher percentages and stated that the flowback water represents 25–90% and 30–80%, respectively, of the injected fluid. These different percentages shows that there is a large uncertainty and range in the amount of flowback volume, which is linked to the difference between geological formations. This in turn means that the amount of fluid returned is site dependent.

Horizontal drilling in the shales is an innovative technology which gives access to more resources in the rock from each well *(Vidic et al., 2013; Jacoby, O'Sullivan and Paltsev, 2011; Stephenson, Valle and Riera-Palou, 2011)*, as the horizontal drilling technique has more reservoir contact, than possible with vertical drilling. According to Vidic et al. (2013) one single well pad at the surface, can contain multiple horizontal wells, which have access to as much as one square mile (~2.59 km^2) of shale that is located more than a mile below the surface. The horizontal drilling technique was introduced in 1929 and fracking was already introduced in the 1940's *(Vidic et al., 2013)*, but it is the combination that gave rise to the Shale Gas Boom. Due to the fracturing of the shale, the permeability and porosity in the rock increases, making it easier for gas to be released and exploited. This makes producing resources from shale gas sites more economical than before.

1.2.2 Environment

Unfortunately the technique of fracking combined with horizontal drilling in shale formations does not come without negative consequences. The biggest and most publicized concern for shale gas production is the many risks and impacts it could bring to the local nvironment. These negative consequences for the environment are mostly caused by the amount of water that is injected into the subsurface, also releasing a lot of chemicals, which in turn can cause heavy metals to be mobilized from the host rock. The production of shale gas requires the use of wide areas of land and high volumes of water. Politics and communities utter their concerns about air quality, water quantity and quality, and also about land and habitat fragmentation *(European Commission, 2014; Vidic et al., 2013).*

One of the greatest concerns for the local environment are the risks related to regional water quality *(European Commission, 2014; Vidic et al., 2013; Environmental Protection Agency, 2012; Mohajan, 2012; Howarth, Ingraffea and Engelder, 2011)*. This is an issue which all reports and papers agree on with one another. As stated above, a large amount of water is injected into the subsurface, along with a fraction of chemicals, during the process of hydraulic fracking. The amount of water injected varies per shale gas site, but approximately two million to seven million gallons (~7.6 million to 26.5 million liter) of water is needed per horizontal well in a shale gas formation to fracture the shale *(Vidic et al., 2013; Environmental Protection Agency, 2012)*. This means that taking an average of about 20 million liter fracking fluid injected per well, indirectly also means that there is about 200,000 liter (2%) of chemicals injected into the subsurface as well. An amount of 2% does not sound small anymore when using such large amounts of fluid.

As water is crucial for all life on Earth, the biggest concern regarding the water quality due to hydraulic fracking is the contamination of the ground and surface water near the area of shale gas production. The chemicals used in the fracking process, which are injected into the subsurface, form the greatest threat of contaminant. Fracking poses risks to ecosystems and human health as the process of fracking extracts hydrocarbons, heavy metals, salts and radioactive materials from the shale *(Howarth, Ingraffea and Engelder, 2011)*. Most studies claim that contamination of the ground and surface water can take place through blowouts, surface spills, leaks from storage facilities, transportation spills, leaks from well casing, leaks from fractured rocks (induced fractures but also from existing faults, or due to improper disposal of fracking fluids *(Ferrer and Thurman, 2015; European Commission, 2014; Vidic et al., 2013; Mohajan, 2012; Nicot and Duncan (2012) Howarth, Ingraffea and Engelder, 2011)*. The main effect of the contamination of ground and surface water, is seen on human health, but also on soils, animals and freshwater organisms. Freshwater from aquifers near an active shale gas production site, are contaminated and cause drinking water unfit for public use. The substances in the contaminated water can cause cancer and other health issues *(Mohajan, 2012)*.

Another problem of water contamination, occurs due to the methane itself as this has been shown to migrate from the shale formation to groundwater in several studies *(Ferrer and Thurman, 2015; European Commission, 2014; Vidic et al., 2013; Mohajan, 2012)*. Gas is often found in water wells, as methane does not only form at depth by the maturation of organic matter, but also at shallow depths through bacterial processes. There is however a difference in concentrations in the natural contamination of water by biogenic methane, and in "shale gas site" water contaminated with thermogenic methane. According to the European Commission (2014) the concentration can be six times higher in water with thermogenic methane than in normal water, which is contaminated by biogenic methane. Reported effects of water contamination by methane differ. While Vidic et al. (2013) states that the concentration of methane can, in extreme cases, cause an explosion, Mohajan (2012) states that the contamination of methane harms human health although he does not describe how Vidic et al. (2013) explains how an explosion can take place; when methane degasses, it can create turbidities and, in extreme cases, explode.

The amount of water used per shale gas site brings a second concern forward for water management, as it can deplete local ecosystems. The water used for fracking is often taken from local sources, as transportation from areas further away costs more money and energy. This depletion in local sources can form a threat to the drinking water supplies in the area, but can also damage freshwater ecosystems and wildlife habitats *(Rahm and Riha, 2012)*. When

local sources near a production site are used for fracking, the contamination of water becomes more severe, as there is less water in the area that can dilute the chemicals (European Commission, 2014).

Another great concern in the environmental risks of hydraulic fracking, is the effect of shale gas production on the greenhouse gas (GHG) emissions. This problem comes with two contradictive parties, where one party states that the GHG emissions of shale gas production is much worse compared to conventional gas production, and where the other party claims that shale gas production releases just a slight bit more GHG emissions than conventional gas production. Methane is a powerful GHG and it has a global warming potential that is 25 times higher than CO_2 *(European Commission, 2014; Howarth, Ingraffea and Engelder, 2011; Howarth, Santoro and Ingraffea, 2011)*. However, methane has a shorter residence time in the atmosphere than CO_2, and therefore its effect attenuates much faster in comparison with CO_2. The main difference in the two parties is the way they look at the GHG emissions; while the opposing party for shale gas production looks at GHG emissions on a scale of 20 years, most papers (which are also more optimistic about shale gas production) looks at GHG emissions on a scale of 100 years.

Beginning with the opposing party, the arguments used for their opinion is that calculations show that the emission percentages of shale gas production is much higher than conventional gas. The emissions of methane into the atmosphere during the life cycle of an average shale-gas well is 3.6–7.9% of the total production of the well, while that of a conventional gas well is 1.7–6% *(Mohajan, 2012; Howarth, Ingraffea and Engelder, 2011; Howarth, Santoro and Ingraffea, 2011)*. This is at least 30% to almost 50% more than that of conventional gas emissions of methane. Howarth, Santoro and Ingraffea (2011) state that it is crucial to take the 20 year horizon instead of the 100 year horizon, as it is necessary to already start reducing the global warming effect in the coming decades and not just over the coming century. The opposing party therefore thinks that the methane emissions of shale gas deserve far greater attention and investigation than it has now, as its effect on a 20 year horizon is much more severe compared to a 100 year horizon. Using shale gas as a bridging fuel to renewable energies over the coming decades would not be advisable according to Howarth, Santoro and Ingraffea (2011), as its GHG footprint is significantly larger than that of conventional gas.

Other reports are a bit more optimistic, saying that the total emissions of shale gas production is only 4–8% higher than conventional gas emissions *(European Commission, 2014)*. The International Energy Agency (2011) even estimate a best and worst case scenario

for the GHG emissions of shale gas production, which are still much lower than the calculations of the opposing party: "… total emissions from shale gas from production through to use (well-to-burner) are only 3.5% higher in the best case (flaring the gas) than the equivalent figure for conventional gas, and about 12% higher in the worst case (venting the gas)." Stephenson, Valle and Riera-Palou (2011) found that with their modelling work the emissions of shale gas production is only approximately 1.8–2.4% than conventional gas, without taking methane emissions into account. However, they state that even for the most unfavourable circumstances and taking efficient flaring of methane releases, the emissions will not be more than 15% higher than those of conventional gas. The authors of the above papers do suggest that the oil and gas industry should take steps to reduce air emissions, by capturing or flaring methane, but also that shale gas is a bridge to a low carbon future if we reduce our coal production and convert motors from diesel to natural gas. Nevertheless, as Jacoby, O'Sullivan and Paltsev (2011) state, "treating gas as a bridge to a lowcarbon future, it is crucial not to allow the greater ease of the near-term task to erode efforts to prepare a landing at the other end of the bridge".

1.2.3 EU-policy

The enormous increase of natural gas due to shale gas production in the United States blew over to Europe, along with its environmental consequences. The difference between the U.S. is that the development of shale gas in Europe is still in an early stage. A lot of political resistance, which is linked to the environmental problems that hydraulic fracking brings, causes limited development in the member states of the European Union *(Slingerland et al., 2014)*. Each member state of the EU is free to decide to explore shale gas, which means that the national governments of each country can decide if their country will participate in shale gas exploration. For some countries (United Kingdom, Poland and Ukraine) this is a positive development as the explorations in shale gas gains in employment, economics and national security *(Howarth, Ingraffea and Engelder, 2011)* and for this reason allowed production of shale gas to commence. But for others (France and Bulgaria) the environmental risks and uncertainties of shale gas production is too great and therefore the governments decided to ban the development of shale gas *(European Commission, 2014)*. A lot of national governments of the EU have also imposed a temporary moratorium on the production of shale gas, so that more research can be done in the meantime, and to eventually decide if their country will contribute with the shale gas development in the EU.

The Netherlands have a few sites which could be interesting for shale gas production and, according to the Rijksoverheid, the estimates of the amount of shale gas in the Netherlands,

range from 200-500 billion cubic meters. For this reason the Dutch government wants to know more about the potential economic effects on the Netherlands of international, or domestic, shale gas production, before giving a licence to start production *(Slingerland et al., 2014)*. The government decided this after they had already given exploration permits to Cuadrilla in 2009 and 2010 and some test wells were also already planned in Boxtel *(Vos, 2014)*. Up to now research is conducted to find out if the environmental risks are low enough and the profit high enough for the Netherlands to start production. Until this research is completed the Netherlands has imposed a moratorium on the production of shale gas.

Germany can only contribute to about 14% of its own demand of natural gas and therefore in 2010 the largest shares of gas imports to Germany came from Russia, Norway and the Netherlands *(SRU, 2013)*. According to the Federal Institute for Geosciences and Natural Resources (BGR), Germany contains an amount between 70 and 230 billion cubic meters of shale gas, which is a great amount and would cause a decrease in the amount of gas needed to import into Germany. The actual recoverable amount would be about 2–7 times the German natural gas reserves from conventional reservoirs *(Vetter, 2015)*. In the beginning of 2014 the production of shale gas was banned as the use of the chemicals in fracking fluid is against their environmental policy.

The United Kingdom has already granted exploration license to Cuadrilla to explore shale gas. The Royal Society and Royal Academy of Engineering have done research about the risks of fracking and concluded that all risks (health, safety and environmental) can be managed effectively in the UK. Nevertheless, they also state that more research should be conducted to find out the GHG footprint that shale gas has. At the moment drilling for shale gas is not yet for commercial use, but does take place in the exploratory phase *(White et al. 2015)*.

1.3 Purpose of this study

The present day challenge for the oil and gas industry is to combine the continued use of fossil fuels while simultaneously reducing the associated CO_2 emissions *(Elliot and Celia, 2012)*. Enough energy needs to be produced to maintain the current standard of living without causing global warming via increased CO_2 emissions due to the production of fossil fuels *(Marcon and Kaszuba, 2015)*. A way of combining these factors is by using carbon capture and geological sequestration (CCGS). CO_2 is being examined as a new fracking fluid to find out if it can be more efficient for industry, by increasing the porosity and permeability of a shale to a higher level compared to the “normal” fracking fluid. Using CO_2 as a fracking fluid and injecting it

into the subsurface would also be a useful way to lower anthropogenic CO_2 emissions by serving as a geologic carbon sequestration (GCS) strategy *(Marcon and Kaszuba, 2015)*.

The efficiency of the fracking processes is dependent on the retention of permeability generated through fracturing. However, reaction of the host shale rock with the fracking fluids ("normal" fracking fluid and CO_2-fluid) or brine can also cause the formation of new phases, such as swelling clays and precipitation minerals (both clays and carbonates). These new phases can block porosity and lead to sudden reductions in production rates. This project addresses the following research question:

Is CO_2-fluid suitable as an environment-friendly way of fracking and does it generate a higher porosity and permeability in shale gas sites, compared to the industrial ("normal") fracking fluid?

The research question will be underpinned by a few research tasks that will help answering the research question. These research tasks are as follows:

1) How does the mineralogy of the shale rock change after reaction with fracking fluid, CO_2-fluid or brine?
2) Does the reaction with fracking fluid, CO_2-fluid or brine increase porosity in shales?
3) Do precipitated phases, e.g. clays, have a positive or negative impact on porosity generation in shale?

To examine the research question and tasks, this project studies changes in porosity and mineralogy at the nanoscale associated with the reaction of shale with brine for comparison with samples reacted with different fracking fluids (CO_2-fluid and "normal" fracking fluid). This will be done using the Tabletop Scanning Electron Microscopy (tabletop-SEM) and Focused Ion Beam-Scanning Electron Microscopy (FIB-SEM). The FIB-SEM will also be used to get 3D-slices of the pore space in these unique shale samples.

The samples investigated in this study, have already been produced by the group of Dr. Kaszuba at the University of Wyoming who are currently conducting experiments on samples from a US based shale gas site. The samples studied in this project come from the Gothic Shale of the Hermosa Group in the Paradox Basin of Utah and Colorado, and are an excellent organic-rich hydrocarbon source rock.

.

2. BACKGROUND

2.1 Geological Setting

The samples investigated in this study are rocks that come from the Paradox Basin, in the Greater Aneth field in southeast Utah. The Paradox Basin is part of the Hermosa Group located in Colorado and Utah, and is an asymmetric basin formed during the Pennsylvanian and Permian time. The basin has an outline that is roughly elliptical with a major axis striking in a northwestern direction *(Hanshaw and Hill, 1969)*. Pacheco (2013) gives estimates of the maximum northwest-southeast length of about 190 miles, and a northeast-southwest width of approximately 95 miles, which is about 306 km and 153 km respectively. It developed along the southwestern flank of the basement-cored Uncompahgre uplift during the Ancestral Rocky Mountain orogenic event *(Lawton and Buck, 2006; Barbeau, 2003; Goldhammer, Oswald and Dunn, 1991)*. During the Uncompahgre uplift, the Paradox Basin was subsiding.

The Paradox Basin is known for its prolific oil fields, like the Greater Aneth, which has produced over 440 million barrels of oil *(Pacheco, 2013)*. The rock that contributes the most to the Greater Aneth oil and gas field, is the Pennsylvanian Desert Creek Limestone *(Marcon and Kaszuba, 2015)*, which is an evaporitic carbonate sequence. Above the Desert Creek Limestone reservoir, lay the organic rich shale layers, the Gothic Shale and the Chimney Rock Shale, which seal the hydrocarbon reservoir rock below (see figure 1).

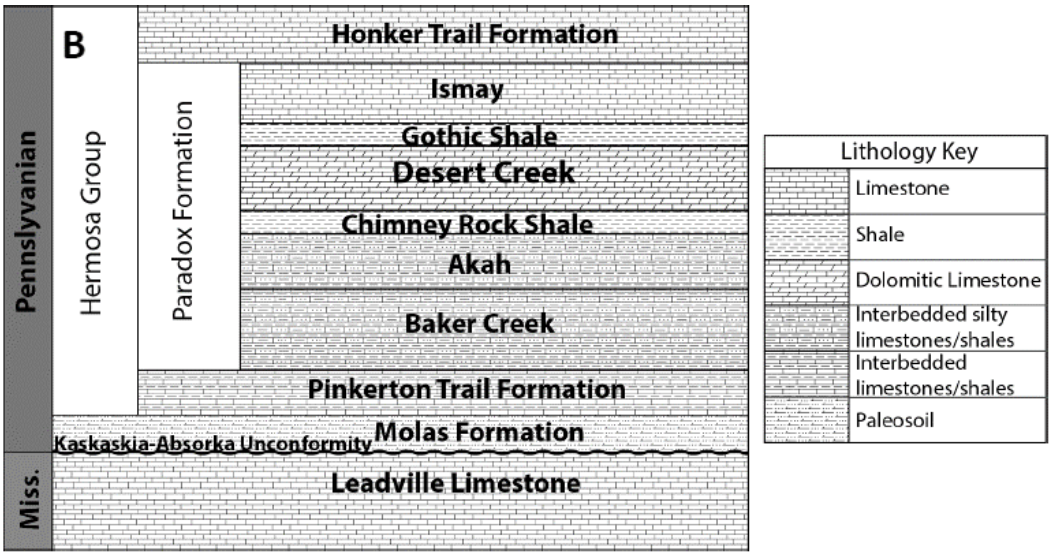

Figure 1. A generalized stratigraphic column of the formations found within the Greater Aneth Field in the Paradox Basin. This study focuses on samples that come from the Gothic Shale, which acts as an organic rich caprock for the main hydrocarbon reservoir rock, the Desert Creek Limestone. Figure comes from Marcon and Kaszuba (2015).

The Paradox Basin was first proposed, by Stevenson and Baars (1986), to have developed by a pull-apart basin formed primarily by right-lateral extension, along two northwest-southeast oriented great faults *(Barbeau, 2003; Goldhammer, Oswald and Dunn, 1991)*. The new idea by Barbeau (2003), is that the basin resembles an intraforeland flexural basin more than a pull-apart basin. Barbeau (2003) states this as the shape, subsidence history, facies architecture, and structural relationships found in the Paradox Basin are exemplary of typical "immobile" foreland basin systems. The latter idea of an intraforeland flexural basin is adopted by the more recent reports, such as Trudghill (2011) and Lawton and Buck (2006).

The basin contains thick deposits of carbonate (dolostone and calcite), salt (halite and anhydrite), black shales and clastics *(Jung, Um and Kirk, 2013; Pacheco, 2013; Heath et al., 2011; Trudgill, 2011)*. The reason for its diverse lithology is that the basin was deposited as a series of glacio-eustatically driven cycles *(Goldhammer, Oswald and Dunn, 1991)*. Throughout the Pennsylvanian time, the basin continued to subside and deposited thick sequences of evaporates (the Paradox Formation) in the foreland basin, along with coarse clastics in the foredeep and carbonates around the basin margins (see figure 2; *Pacheco, 2013; Trudghill, 2011; Lawton and Buck, 2006; Barbeau, 2003; Hanshaw and Hill, 1969).*

2.2 Gothic shale

As already stated, the rocks used for this study are from the Gothic Shale deposition. The Gothic shale found in the Paradox Basin is one of the black shales deposited during the Pennsylvanian time, during a euxinic-evaporitic phase. It represents the maximum flooding surface for the third cycle of the Paradox Member and occurs across the entire Paradox Basin *(Pacheco, 2013)*. It overlies the Desert Creek hydrocarbon-producing zone of the Greater Aneth Field. The Gothic Shale is mature, containing type II and mixed type II-III kerogen *(Pacheco, 2013; Heath et al. 2011)*. It is a remarkably uniform, black to gray, laminated to thin-bedded, dolomitic marine shale *(Jung, Um and Kirk, 2013)*. Goldhammer et al. (1994) described the Gothic Shale as a deposition of a transgressive systems tract (see figure 2), which contains sapropelic dolomite to silty carbonate mudstone. At the Greater Aneth Field the Gothic Shale has a thickness ranging from 1.5-8.2 meters *(Jung, Um and Kirk, 2013; Heath et al., 2011)*, and generally thins out over the (Desert Creek) carbonate buildup complex.

The textural and mineralogical components in the Gothic Shale include silt-sized quartz, calcite, dolomite, and mica in a dominant clay matrix (predominately montmorillonite, which belongs to the smectite group) as the major mineral phases, along with the presence of

authigenic pyrite *(Marcon and Kaszuba, 2015; Jung, Um and Kirk, 2013; Pacheco, 2013; Heath et al. 2011)*. The other clay minerals present in the shale are discrete illite, chlorite, corrensite and mixed-layer chlorite-trioctahedral smectite *(Pacheco, 2013)*. Heath et al. (2011) took four core samples to measure the average porosity, pressure-decay permeability, and total organic content (TOC) of the Gothic Shale; this turned out to range from 2.7–4.3% , 1.3×10^{-19} – 1.4×10^{-19} m^2, and 2.2–4.4 wt% respectively.

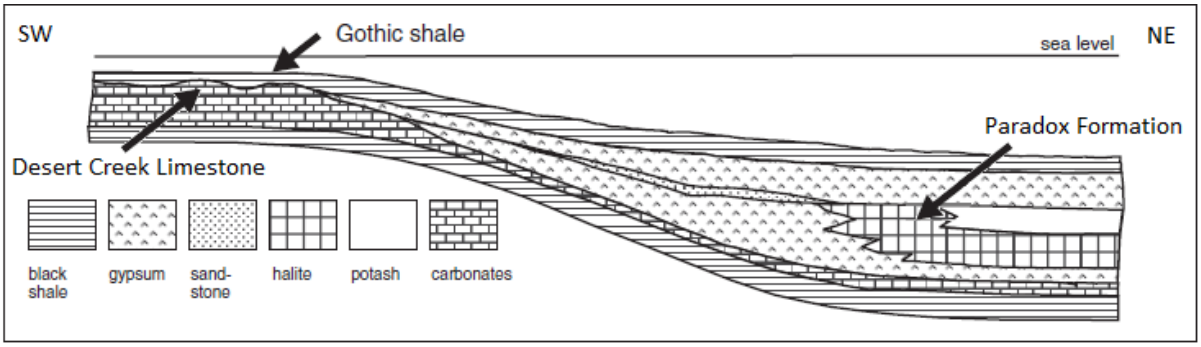

Figure 2. Cross section showing the transgressive system tract that deposited the Gothic shale (at the Greater Aneth Field) or black shale facies over the shelfal carbonates (like the Desert Creek Limestone). It can be seen that from the deepest part of the basin (NE) toward the basin shelf (SW), the amount of evaporates in the cycle diminishes, while the percentage of carbonates increases. The water depth was estimated as >35 m. Figure comes from Heath et al. (2011) who modified it from Goldhammer, Oswald and Dunn (1994)

3. THEORY OVERVIEW

The theory overview section is written to describe the difficulties encountered when dealing with shale gas, especially when fluids are involved. Shales contain clay minerals, which can swell when they come into contact with water or other fluids. This is a bad thing for the oil/gas industry as it will cause a decrease in the porosity and permeability of a shale, making it harder to extract gas or oil from the shale. Another thing to keep in mind when considering shale, is that shale is a nanocomposite material. This means that Darcy's law is not applicable for shales and new laws/equations are needed to define the flow transport in a nanocomposite shale. Both of these problems will be described in this section.

3.1 Swelling clays

Shale is a mudstone, which is characterized by its fissility, meaning that it splits easily into thin layers along the closely spaced, roughly planar and approximately parallel bedding planes. Mudstones, and thus shales, contain a high amount of clay minerals. Clays are layered minerals, classified among the phyllosilicates, and formed during the processes of weathering and decomposition of igneous rocks *(Anderson et al., 2010)*. All kinds of different clay minerals exist, varying in their layer arrangement, substitutions and composition. They can generally be classified by structure as allophone, kaolinite, halloysite, smectite, illite, chlorite, vermiculite, attapulgite–palygorskite–sepiolite and mixed layer minerals *(Grim, 1968* cited by *Anderson et*

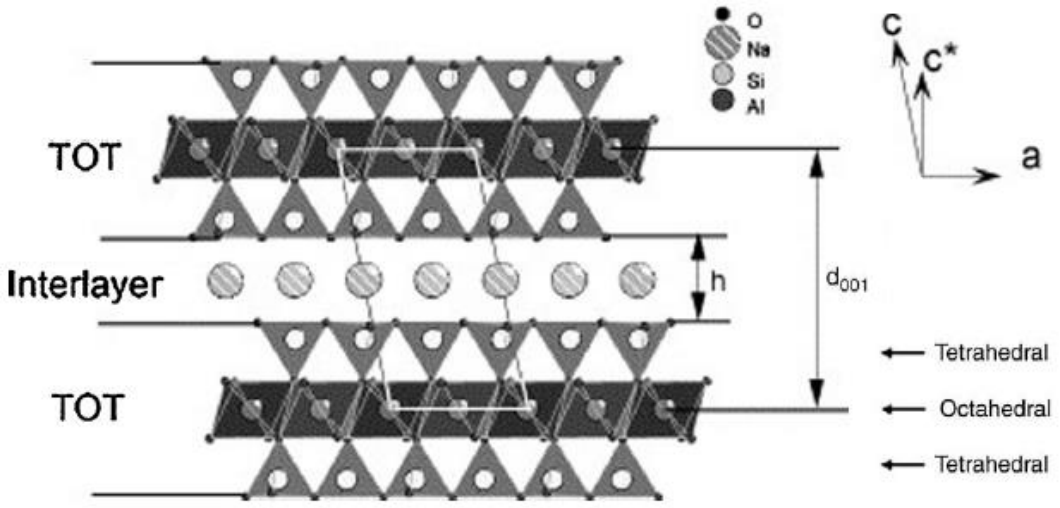

Figure 3. The 2:1 layered structure and basal unit cell dimension of smectite clay minerals, showing an octahedral silicate sheet sandwiched between two tetraherdral silicate sheets. The space between the 2:1 structures lies the cation-filled and generally hydrated interlayer region. The d_{001} distance resemples the basal interlayer spacing, which increases with higher hydration states. Figure comes from de Jong, Spiers and Busch (2014)

al., 2010 and *Chen et al., 2008).* The naturally occurring clay minerals consist predominantly of stacks of two-dimensional aluminosilicate sheets, which carry a negative charge *(Anderson, 2010; Chen et al., 2008).* The aluminosilicate layers consists out of tetrahedral and octahedral sheets. The octahedral sheets are formed by Al^{3+}, Mg^{2+} or Fe^{3+} oxides, while the tetrahedral sheets consists out of Si^{4+} oxides *(Anderson et al., 2010).* The lattice structure of a clay can either be composed of a single silica tetrahedral sheet joined to a single octahedral sheet (referred to as a 1:1 clay or a T–O clay), or it can be composed by two silica tetrahedral sheets sandwiching a single octahedral sheet (referred to as a 2:1 clay or as a T–O–T clay).

Between two aluminosilicate layers, there is an interlayer space (see figure 3), with widths in the nanometer scale. As the aluminosilicates are negatively charged, the interlayer must contain species which are positively charged to compensate the aluminosilicate layer. This positively charged interlayer along with the van der Waals attraction of the water molecules, hold the aluminosilicate layers very strongly together *(Hensen and Smit, 2002; Madsen and Müller-Vonmoos, 1989).* The cations in the interlayer of a clay are exchangeable and may therefore trade places with other cations under the appropriate conditions. Pinnavaia (1983) described these conditions as the cation exchange capacity of a clay, which is dependent on its crystal size, pH and the type of exchangeable cation. The exchangeable cations are an important property of clays as it affects the interaction between organic molecules and the clay. The cations in the interlayer determine the likelihood of intercalation or exfoliation of molecules into or out of the clay's lattice, and therefore provide opportunities to adjust the surface energy and the interaction with organic species *(Chen et al., 2008).* This property of clay can cause clays to swell (hydration) or to collapse (dehydration). It should be noted that the swelling of clays is a fully reversible process *(Madsen and Müller-Vonmoos, 1989)*

When studying swelling clays, studies are mainly focused on smectite clays due to their large swelling potential and due to the frequency with which they are encountered during drilling operations *(de Jong, Spiers and Busch, 2014; Anderson et al., 2010; Chen et al., 2008).* The reason why smectites are more prone to swell than other types of clay, is due to their capacity to host water and organic molecules in their interlayer spacing, high capacity for cation exchange, high aspect ratio and large surface area *(Chen et al., 2008)*. The smectite group has the structure of a 2:1 clay (see figure 3) and incorporates a variety of clays, such as montmorillonite, bectorite and beidellite. These clays are common minerals in caprocks and faults sealing potential storage reservoirs, found at depths up to about 2–3.5 km, with temperatures up to 100˚C *(de Jong, Spiers and Busch, 2014)*. Beyond these conditions, smectites often start to transform to the non-swelling clay mineral illite. For this study it will

be interesting to find out what happens to the samples, as the Gothic shale contains both the swelling clay smectite (montmorillonite) and the non-swelling clay illite.

3.1.1 Through exposure with H_2O

The interlayer materials of a swelling clay are easily interchanged with the external environment, making these clay minerals distinguishable from other non-swelling clays *(Giesting et al., 2012a)*. As stated before, the amount of water uptake depends on the cation species present in the interlayer. An example of this can be given with the smectite clay montmorillonite; montmorillonite often tends to contain small inorganic species such as Na^+ and Ca^{2+} cations. As the swelling property depends on the nature of the cations, these two different species have a different swelling pressure, with Ca^{2+} cations resulting in smaller swelling pressures than Na^+ cations.

The migration of water molecules into or out of the interlayers of a clay causes the structure of the clay to expand or to contract. This is dependent on factors such as temperature, pressure, water activity and clay composition *(de Jong, Spiers and Busch, 2014)*. When the interlayer takes up water molecules, expansion takes place, resulting in the swelling of clay. In swelling clays, two phases of swelling can occur; the first phase occurs by intracrystalline swelling and the second phase by osmotic swelling. In short, intracrystalline swelling is caused by the hydration of the exchangeable cations of the dry clay, while osmotic swelling results from the large difference in the ion concentrations close to the clay surfaces and in the pore water *(Madsen and Müller-Vonmoos, 1989).*

Intracrystalline swelling is the first step in the swelling process of a clay *(Schädlich, Marcher and Schweiger, 2012; Madsen and Müller-Vonmoos, 1989).* Before water is incorporated into the clay, the cations in the interlayer of a dry clay are located on the surface of the aluminosilicate sheets, or positioned in the hexagonal holes of the tetrahedral sheets. When these cations come into contact with water molecules, they order themselves in the interlayer between the two aluminosheets, causing the dry clay to become hydrated *(Madsen and Müller-Vonmoos, 1989)*. This process leads to the widening of the interlayer, automatically also widening the d_{001}-spacing (see figure 3). Intracrystalline swelling acts over very small distances (up to 1 nm). Osmotic swelling can act over larger distances compared to intracrystalline swelling.

Osmotic swelling takes place after a clay is already hydrated, as it needs water molecules to cause an ion concentration difference. It results from the large difference in concentration between the ions electrostatically held close to the clay surface and the ions in the pore water

of the rock (see figure 4a.) *(Madsen and Müller-Vonmoos, 1989).* After the cations aligned themselves in the interlayer at the surface of the clay sheets and are surrounded by water molecules, they form a so called electric double layer along with the negatively charged clay sheets *(Schädlich, Marcher and Schweiger, 2012; Madsen and Müller-Vonmoos, 1989).* Looking at the interlayer, this means that at the surface of the clay sheets the positive ion concentration is extremely high, and decreases with increasing distance from the surface. The exact opposite is seen with the negative ion concentration, which is low at the surface of the clays, but increases with decreasing distance from the surface. In figure 4b it can be seen how the negatively charged clay surface and the cloud of ions form the diffuse electric double layer. It also shows how the negative potential of a clay sheet is the largest near the particle surface and decreases in the ion concentration layer to zero at the pore water boundary. When two negative potential fields overlap each other (meaning that two negatively charged aluminosilicate sheets come too close to each other), they repel each other, which causes an increase of the interlayer distance due to water that is drawn into the interlayer, resulting in further swelling of the clay. According to Madsen and Müller-Vonmoos (1989) the profile of the potential curves, which also means the repulsion at a given distance, vary with the valence and the radius of the counter-ions in the double layer and with the concentration of electrolytes in the pore water.

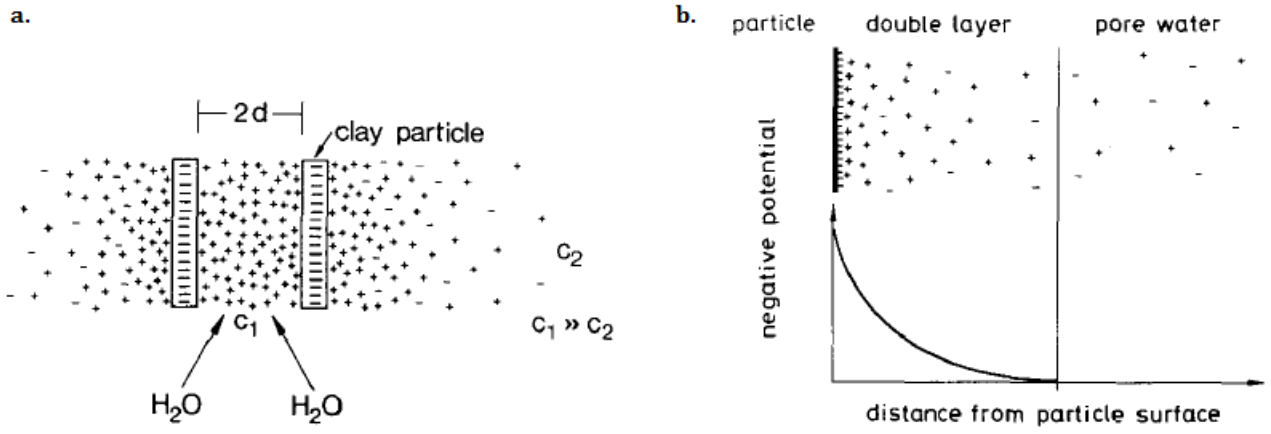

Figure 4a. Two negatively charged clay layers with ion cloud. The ion concentration C_1 between the layers is much higher than the ion concentration C_2 in the pore water. An equilibration of the concentration can only be reached through the penetration of water into the space between the clay particles (thus in the interlayer) *b.* Negatively charged clay surface, ions in the diffuse double layer and ions in the pore water. The distribution of the negative potential of a clay particle changes with the valence and the radius of the ions in the double layer and with the electrolyte concentration in the pore water. The negative potential field is the largest near the particle surface, and decreases to zero at the pore water boundary. Both figures come from Madsen and Müller-Vonmoos (1989).

3.1.2 Through exposure with CO_2

While a lot of research has been conducted on the water uptake and swelling properties of (smectite) clays, there has only been a few studies directed at the possible interactions of swelling clays with CO_2 under conditions that are typical for geological storage *(de Jong, Spiers and Busch, 2014)*. In an era where GHG emissions into the atmosphere are increasing, new ways are investigated for anthropogenic CO_2 sequestration. Injecting CO_2 into deep geological formations is regarded as a possible solution for long-term storage of carbon dioxide and reducing the anthropogenic GHG emissions. There are enough geological storage options such as saline aquifers, depleted gas and oil reservoirs or unminable coal seams *(Busch et al., 2008)*. Before applying this relatively new method, we must understand the processes occurring and long-term behaviour when CO_2 is injected and slowly migrates into the low permeability pore network present in caprocks and faults *(de Jong, Spiers and Busch, 2014; Giesting et al., 2012a; Busch et al., 2008)*.

According to Giesting et al (2012b) the injected CO_2 will react with the contents of the deep geological formation, both as the pure phase and as carbonate dissolved in groundwater. The only question is 'how will the CO_2 react with the geological formation?'. CO_2 can either react with the sealing caprock which will eventually cause the clay in the impermeable caprock to swell (decreasing the porosity and permeability), and keeping the injected CO_2 in the geological reservoir. Or the CO_2 can cause the clay to collapse (increasing the porosity and permeability), resulting in an eventual release of CO_2 back into the atmosphere. An understanding of these processes, and the risks and rates of possible leakage is needed for site approval, public acceptance and the awarding of credits for stored CO_2 quantities *(Busch et al., 2009; Busch et al., 2008)*

Busch et al. (2008) investigated sorption and diffusion measurements of CO_2, to evaluate and understand the molecular transport through and the sorptive storage behaviour of a well-defined regional caprock and a variety of clay minerals. Their shale sample studied, coming from the Muderong Shale, showed that the sorption capacity of CO_2 is entirely attributed to its clay mineral contents. Busch et al. (2009) agrees with this, and goes further in looking at the individual clay minerals present in shales (smectite, illite, kaolinite and chlorite). Their sorption experiments demonstrated that the CO_2 sorption capacities decrease with decreasing micropore volumes in the order (from high micropore volume to low micropore volume); smectite, illite, kaolinite and chlorite. Busch et al. (2008) also showed that illite and kaolinite (non-swelling

clay minerals), are also able to absorb significant amounts of CO_2, while these minerals are not known for interlayer expansion under any experimental conditions.

Another result of Busch et al. (2008) is that geochemical alterations due to the reation with CO_2, such as dissolution of silicate and precipitation of carbonates, may also have a measurable effect on the porosity, permeability and diffusion properties of shales, which can enhance the transport properties in the shale. Their final conclusion is that CO_2 injection causes a positive view on the sealing integrity of the intact caprock formations, as it will immobile the pore network of the caprock.

Giesting et al. (2012a) examined Na-exchanged montmorillonite under pressure using in situ X-ray diffraction. Their study found that clays swell up to approximately 10% when in contact with CO_2 at pressures from 50-640 bar and temperatures of 22−45°C. These results suggest that CO_2 can migrate into the clays interlayer, causing the clays to swell. Giesting et al. (2012b) did a somewhat similar research, but looked at K- and Ca-exchanged montmorillonite. Both types of montmorillonite swell upon interacting with CO_2 at ambient temperatures. The difference between the two samples is that K-exchanged montmorillonite expands rapidly, while the Ca-exchanged montmorillonite swells more slowly.

De Jong, Spiers and Busch (2014) did a similar study as Giesting et al. (2012a) on Na-montmorillonite at PT conditions expected in relatively shallow CO_2 storage reservoirs; pressure of 15 MPa (150 bar) and temperatures around 45°C. Their aim was to obtain accurate "whole rock" swelling data, compared to only obtaining diffraction data on d-spacing changes like the research of Giesting et al. (2012a) did. This resulted different findings for the amount of swelling where the penetration of CO_2 into the clay's interlayer, caused only minor swelling of clay up to 3%. This amount can close small fractures or joints and thus reduces the bulk permeability.

An important and unexpected result that the papers above all have in common is the finding that the amount of CO_2 sorption capacity depends on the initial hydration state *(de Jong, Spiers and Busch, 2014; Giesting et al., 2012a; Giesting et al., 2012b; Busch et al., 2009; Busch et al., 2008)*. The CO_2 sorption capacity decreases with decreasing moisture content. The reason why this is an unexpected finding, is that it is always believed that water molecules compete with CO_2 for sorption sites. This would make you expect lower CO_2 sorption capacities for moist samples, instead of the higher sorption capacities found.

Kang et al. (2011) suggested that storage of CO_2 in organic-rich shales has added advantages as the organic matter acts as a molecular sieve. CO_2 molecules can therefore reside in small pores that the other naturally occurring gasses cannot access. Added to this, CO_2 is

more easily and enhanced adsorbed compared to other gasses, as the molecular interaction energy between the organics and CO_2 molecules is different. Therefore the affinity of shale to CO_2 is partly due to steric and thermodynamic effects (Kang et al., 2011).

3.2 Transport mechanisms and nanopore chemistry

In geochemisty, the nanometer (1 nm=10^{-9} m) scale plays a vital role in the understanding of many key geochemical processes *(Wang, 2014)*, and will provide a link between the molecular-level understanding and the macro-scale laboratory/field observations. One of these processes mentioned by Wang (2014), which is relevant for this study, is that the nanometer-sized pores in shales, directly control the gas disposition and release in shale gas sites.

As already stated before, the conventional oil and gas reserves are depleting, and therefore it is necessary to turn to unconventional oil and gas reserves. An important difference between unconventional and conventional gas reservoirs, is that unlike conventional gas reservoirs, gas flow in shale reservoirs is a complex and multi-scale flow process which has special flow mechanisms *(Guo et al., 2015)*. To economically produce hydrocarbons from unconventional oil and gas sites, the industry must understand the workings of the flow process and pore structure of a low-permeability rock, such as shale *(Chalmers, Bustin and Power, 2012)*. The knowledge of conventional reservoirs is not applicable to shale gas formations.

3.2.1 Fluid flow in nanopores

The reason why more studies are done to understand the emergence of new properties of nanostructured matericals, is because the properties of a material can deviate drastically from those of the corresponding bulk phase and become size-dependent *(Wang, 2014)*. Wang (2014) states that physical or chemical properties emerge when the size of the material is reduced in at least one dimension to nanometers. Nanopores are abundant in geological formations and when a fluid flows through a nanopore, it can behave differently from its bulk phase. The discrete nature of molecules become much more important when a fluid flows through a nanometer channel, as it contains much less molecules than when it flows through a macroscopic system *(Wang, 2014)*. A dimensionless parameter, called Knudsen number (Kn), is introduced to correct for Darcy's equation which is not applicable anymore on fluid flow and transport in nanochannels.

Knudsen number is described in a formula as: $Kn = l/L$, where L is the characteristic length of a fluid flow system and l is the mean free path of a molecule for a gas or the interaction

length of a molecule with its neighbours for a liquid *(Wang, 2014)*. In table 1, it can be seen how Ziarani and Aguilera (2012) use the Knudsen number to classify flow regimes. In short they state that for Kn < 0.01, a continuum (viscous) flow dominates and Darcy's equation is applicable. For Kn values between 0.01 and 0.1 a slip flow dominates applying Darcy's equation with the Klinkenberg or Knudsen's correction. In the slip flow regime gas molecules experience slipping at the solid surface *(Wang, 2014)*. For 0.1 < Kn < 10, a transition flow dominates, meaning that it can involve both slip and diffusion flows. When the Kn-value rises up to 10, the traditional flow dynamic starts to fail and the flow regime becomes non-Darcian flow. This means that at Kn > 10, a free molecular flow regime dominates and the Knudsen's diffusion equation is used. The Knudsen's diffusion equation is as follows:

$$\frac{q\rho M}{\phi A} = D_k \frac{\Delta P}{RTL}$$

Where D_k is the Knudsen diffusion coefficient; ρ is the density of gas; M the molar mass; P the pressure of gas; ϕ is the porosity of shale; A the surface area; and L is the diffusion distance.

Table 1. Knudsen number and flow regimes classifications for porous media *(Ziarani and Aguilera, 2012)*

Flow regime	Knudsen number	Model to be applied	Comment
Continuum (Viscous) flow	Kn < 0.01	Darcy's equation for laminar flow and Forchheimer's equation for turbulent flow	Assumes immobile fluid at the pore wall. Hence, no permeability correction is generally required
Slip flow	0.01 < Kn < 0.1	Darcy's equation with Klinkenberg or Knudsen's correction	Knudsen's correction is more accurate, but Klinkenberg's correction is easier and, as a result, is generally implemented
Transition flow	0.1 < Kn < 10	Darcy's law with Knudsen's correction can be applied. Alternative method is Burnett's equation with slip boundary conditions	Knudsen's diffusion equation is a more reliable approach, especially when Kn is closer to 10
Knudsen's (Free Molecular) flow	Kn > 10	Knudsen's diffusion equation.	Usually occurs in shale formations where the pore-throat radius is very small

Ziarani and Aguilera (2012) give an equation for the Knudsen's correction factor used on Darcy's Law:

$$f_c = [1 + \alpha(Kn)Kn]\left[1 + \frac{4Kn}{1 - bKn}\right] = \frac{q}{q_{Darcy}}$$

Where q is the fluid flux; q_{Darcy} is the flow flux calculated from Darcy's Law; α is the rarefaction coefficient, which is a function of Kn; b is a constant equal to -1 for slip flow.

Wang (2014) gives a few properties and processes that should be kept in mind when considering molecular transport in nanopores. The first thing is that when the pore size decreases, the surface-to-volume ratio of a fluid flow system increases making the interfacial effect of enhanced importance. The channel wall of a nanopore is therefore very important when fluid flows through the nanochannel. It determines the behavior of the molecules, when it comes into contact with the fluid molecules. Wang (2014) says that when a polar liquid is in contact with a hydrophobic surface, the attraction among fluid molecules is stronger than that between the fluid molecules and the solid surface. For this reason the fluid molecules try to minimize contact with the solid surface, which leads to an increase in liquid flow velocity compared to the bulk fluid *(Wang, 2014)*.

The second process Wang (2014) explains, is the size exclusion that should be considered in molecular transport in nanopores. Experimental measurements done on coal show that the diffusion rate of CO_2 is usually 1-2 orders of magnitude greater than that for methane (CH_4). This seems to be in contrast with fundamental physical law as CH_4 is lighter than CO_2. This behavior has been recognized to be induced by nanometer-scale pore spaces, as it contains large energy barriers and directional force fields. In the example of CO_2 and CH_4, the CH_4 molecules need to overcome much higher energy barriers in the pore throats, as the size of the pore throat are close to the kinetic diameter of CH_4 molecules. According to Wang (2014) this process may control gas/oil migration and extraction in low-permeability unconventional reservoirs and may also occur in shale gas reservoirs.

The last thing Wang (2014) considers is the surface charge density which is important in regulating fluid and ion transport in nanopores. He found that water molecules experience larger friction at higher surface charge densities, because the water flow decreases with the increase of charge density for both positively and negatively charged channels. Flows increase with increasing channel size, for both water and ions *(Wang, 2014)*.

3.2.2 Shale as nanocomposite material

Shales are known as rocks with natural nanocomposite material, which has a large proportion of clay particles *(Wang, 2014)*. These clay particles contain a significant amount of nanoparticles. Shales do not only contain nanoparticles, but also nanopores. Organic shale has the ability to store a significant amount of methane gas permanently due to its trapping

mechanism. Methane can exist in shales in either a compressed phase or as an adsorbed phase, of which the latter accounts for 20-85% of the total gas-in-place (GIP) (*Wang, 2014)*. This takes place within its finely dispersed organic matter, which is a nanoporous material with mainly micropores (< 2 nm) and mesopores (2–50 nm), mainly trapping methane gas in an adsorbed state *(Kang et al., 2011)*. These micro- and mesopores are extremely important for the gas industry, as it contributes to a large part of the shale porosity and storage sites for sorbed methane. The pore size distribution seems to exhibit a fractal nature, of which it is known that chemical reactions in a fractal medium may react differently from that of a non-fractal medium *(Wang, 2014).*

Methane can be adsorbed to both the clay particles as the organic matter (kerogen) in a shale. The abundance of pores in kerogen has a direct relation to the thermal maturity of the organic matter *(Wang, 2014)*. He suggests that the thermal maturation of kerogen may enhance the methane sorption in shale most likely due to an increase in nanoporosity, while the methane sorption seems to reduce in the presence of moisture. Another thing noticed is that MD simulations indicate that the density and viscosity of methane in a confined environment could deviate significantly from those in the bulk phase, which has the potential to affect the total GIP estimation and overall gas recovery *(Wang, 2014)*. Other properties that depend the behavior of shale gas, is the surface area and the pore throat size in shale. Wang (2014) found that the high surface area attributes to the development of nanometer-sized pores in kerogen, and the pore throat size in shale seems to directly control the hydrocarbon release from the shale matrices. The latter goes hand in hand with the displacement of methane by CO_2, which takes place in two stages. While in the first stage, the co-adsorbed CO_2 may enhance the CH_4 adsorption, in the second stage the stronger affinity of CO_2 to the surface can cause the release of CH_4 molecules from carbon materials *(Wang, 2014)*.

As already discussed in 3.3.1, the way a fluid or gas flows through a nanochannel behaves differently than the bulk phase. The traditional assumptions of no-slip boundary conditions in the Navier-Stokes equation does not apply for nanometer scale pores/channels in a shale *(Wang, 2014)*. The commonly used Darcian flow model also falls short, and needs the Knudsen's correction factor when considering the nanopores in shale, when $0.1 < Kn < 10$ (see table 1). The mechanism in which gas transport takes place within the nanometer-scaled channels of a shale, is through both diffusion (molecular flow), using the Knudsen's equation, and through advection (Darcy flow), using Knudsen's correction factor *(Wang, 2014; Chalmers, Bustin and Power, 2012; Ziarani and Aguilera, 2012)*.

4. METHODS

This project is mostly based on microscopic research at the nanoscale. The analysis steps for the samples reacted with fracking fluids, CO_2-fluid as well as the samples reacted with reservoir brines are the same. The first step was sample preparation. The samples have been embedded in epoxy and cross sectioned so that the outer reacted section of the sample could be identified and compared to the inner, unreacted shale rock. This was a critical step, as this step can make or break the project. After sample preparation was done, the samples were looked at with a tabletop Scanning Electron Microscope (tabletop-SEM). Chemical data has been obtained using Energy Dispersive X-ray spectrometry (EDX) during SEM analysis to find out more about the mineralogy and elements within the samples. Further analysis of the pore space and its connectivity has been done using the Focused Ion Beam-SEM (FIB-SEM). Image analysis was conducted to separate pore-space images in the sample.

4.1 Samples

4.1.1 Background

The samples used in this study have already been produced by the group of Dr. Kaszuba at the University of Wyoming who are currently conducting experiments on samples from a United States based shale gas site. These samples are from the Gothic Shale of the Hermosa Group in the Paradox Basin, located in Utah. Four different type of samples were provided for this study. These four different samples are the following:

1) An unreacted Gothic Shale sample, as it is found in the subsurface
2) Two types of samples of the Gothic shale which were experimentally fracked, using normal (industrial) fracking fluid
    a. One sample which has only reacted with the fracking fluid (EHR-001 *reacted*)
    b. The other sample which is the same as 2a but also washed afterwards (EHR-001 *reacted + washed*).
3) Gothic Shale that was put into a solution containing CO_2-fluid and brine (EPA-1)
4) Gothic Shale sample that was put into a solution which only contained brine (EPA-2).

In total ten samples were provided; one of each of the unreacted Gothic Shale, the EHR-001 *reacted* and the EHR-001 *reacted + washed*; five of EPA-1 and; four of EPA-2. The size of the

samples did not vary a lot from each other. Most were small rectangular blocks with lengths, widths and heights of just a few millimeters.

4.1.2 Preparation

Before putting the samples under the microscope, a sample was put into an epoxy of Araldite 2020 A and B, in the proportion of 100/30 respectively. The unreacted Gothic Shale was the only sample put into this epoxy. This was an important step, because it would not be good for the project if the resin reacted with the sample, as it could alter the samples and make the data unreliable. After the epoxy dried, and the sample was put on a sample holder, it was argon polished and coated with platinum, and ready to use under the tabletop-SEM. The samples that were not put into an epoxy, were put on a sample holder with carbon stickers, and coated with platinum.

4.2 Microscopy

4.2.1 Tabletop-SEM

To examine the samples on the differences in porosity and permeability, the samples imbedded in epoxy as well as the samples not imbedded in epoxy were examined using a JEOL JCM-6000 NeoScope tabletop-SEM. The tabletop-SEM is next to the secondary electron detector, also equipped with a backscattered electron (BSE) and energy-dispersive X-ray (EDX) detector, making analyzing the samples on their mineralogy and porosity easier. The tabletop-SEM was used for overview work and to lay down the basis of this project. The overview done using the tabletop-SEM was to find interesting features on the samples, which could be better investigated using the FIB-SEM.

4.2.2 FIB-SEM

For better quality pictures than the tabletop-SEM and for 3D-analyzation, the samples were also examined with a FEI Nova Nanolab DualBeam Focused Ion Beam-SEM, located at the Center for Electron Microscopy Utrecht (EMU), Utrecht University. This microscope is equipped with both a gallium and electron beam. Most of the EDX analyzes was already done with the tabletop-SEM, but when needed, EDX-analyses were also done using the FIB-SEM.

For 3D-visualization the areas of interest were cut into. Before cutting into the sample, a platinum layer (thickness of 1-2 µm, with a width dependent on the area of interest) was deposited in situ on the surface of a specific location, to protect the area of interest. This is done

to prevent curtaining during the cutting process and so that the ion beam does not destroy the area of interest. After the platinum layer was deposited, the cutting process started by using the 30kV gallium beam with a current of 5.0 nA to cut a depth of 2.0 µm. The low power of 5.0 nA was used just to be safe and protect the area of interest. A 20 nA current was used in front of the area of interest to expose it and get a 3D-visualisation. In figure 5 the process of FIB-SEM cutting can be seen.

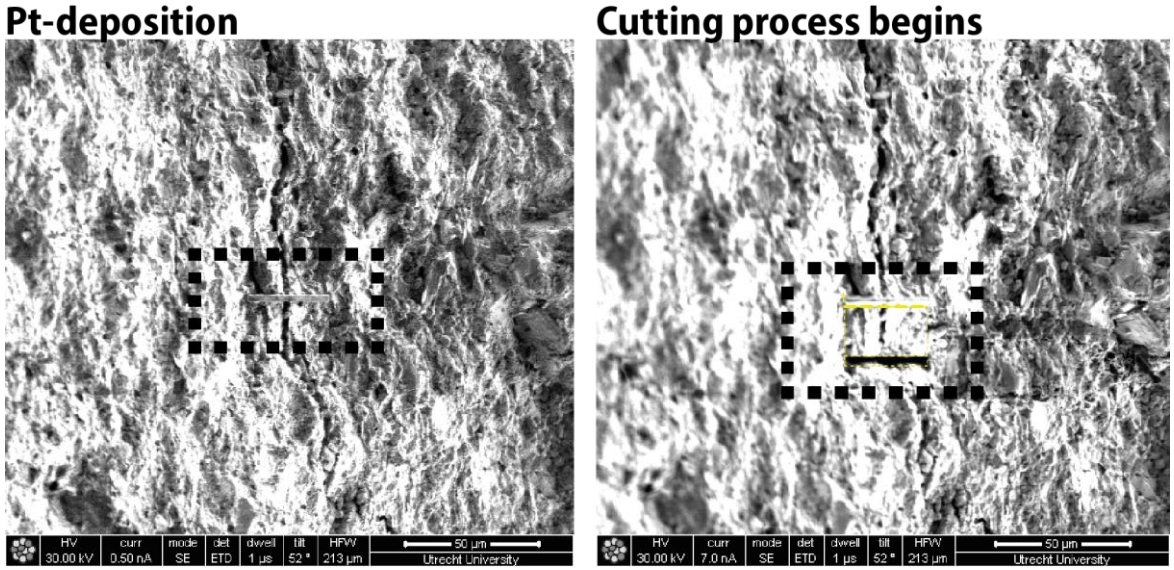

Figure 5. FIB-SEM images to demonstrate how the cutting process works. The area of interest in these figures is a crack found in the EPA-1 (CO_2-fluid) sample. In the left image a thin greyish rectangular can be seen in the black dashed line. This thin, grey rectangular shows where the platinum layer has been depositioned to protect the sample from damage due to the gallium beam. In the right image, it can be seen how the cutting process begins. It starts at the bottom and moves upwards towards the Pt-deposition.

4.3 Image processing and analysis

To process and analyze the data gathered from both the tabletop-SEM and FIB-SEM, ImageJ software (version 1.49p; *Rasband, 2014*) was used. This software helped to get images with different contrast and brightness features at approximately the same contrast and brightness so that comparison would be easier to make between different images. A plugin of the ImageJ software helped to create a large overview of the different samples. For each shale sample, a dozen or more pictures were taken at a certain magnification, to eventually create one large image, which was not possible to see on the microscope screen at the same magnification. This was done with the *ImageJ*™ plugin *Stiching*™ *(Preibisch, Saalfeld, and Tomancak, 2009)*.

ImageJ was also used to find out the sizes of pores and the pore distribution of the different shale samples. This was done by scaling each picture to the scale bar and magnification of the image. After scaling the picture, the image was cropped, so that the scale bar was excluded out

of the image. The reason for doing this, was to prevent the scale bar being seen as a pore space by ImageJ. The image that was left over, was then thresholded to its pore content. When thresholding, I focused on one very clear pore visible in the image, and made sure that this pore was included as a whole while thresholding. This was done for every image, so that the total porosity found would be as consistent as possible. When this was achieved, the threshold was applied and the particles left, were analyzed. Figure 6 shows the process of scaling, cropping and thresholding, to illustrate how the pore size and surface area were measured. Something to keep in mind is that when thresholding the image, some very small pores may be overseen and therefore the total porosity might be underestimated, or the other way around, too many particles are seen as pores, and therefore the total porosity might be overestimated.

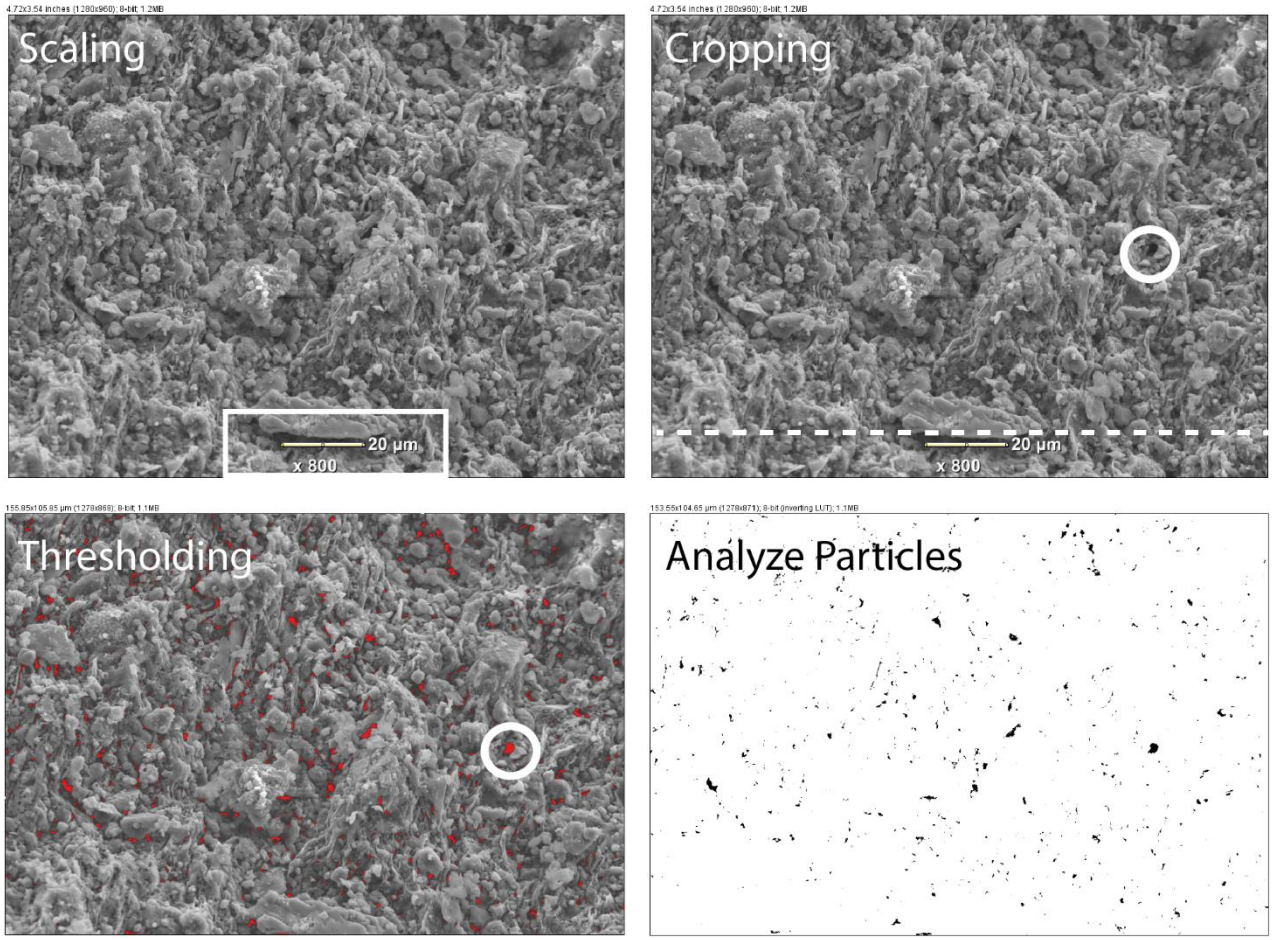

Figure 6. Tabletop-SEM images showing how the amount of pores and pore surface area were measured using ImageJ. In the scaling part (top left) the scale was set to the scale bar, which is in this image 20µm. After doing this, the figure was cropped (top right), to remove the scale bar and the magnification out of the image, so that it wouldn't include that part when thresholding. I focused my attention on a pore that I found the most visible and clear, and while thresholding, I waited till that pore was completely filled (red, seen in the image down left). When applying the threshold, a white image with black spots would be conjured (down right), in which the next step was to analyse those black particles seen.

5. RESULTS

The results section will give the observations of each sample type separately. The industrial fracking fluid samples (EHR-001 *reacted* and EHR-001 *reacted + washed*) will be discussed in a single section, unless big differences are observed between the two, which will then be highlighted separately for the individual samples. Per sample type the mineralogy and structures, porosity and the presence of swelling clays and/or precipitated minerals will be described. For the fracking fluid, CO_2-fluid and brine samples the differences between the bedding plane and the surface of the bedding planes will be given. This will not be done for the unreacted sample as the only sample provided of the unreacted Gothic shale, was put into an epoxy, before looking at the surface and bedding plane properties of the shale.

In the results section four different magnifications will be used in the text, in table 2 and in figure 13 (x300, x600, x850 and x1500). The reason for this is that most images taken were done at these four magnifications, making it easier to compare the four types of samples to one another. When describing the samples, the description will either be about the "surface" of a sample, or about the "bedding (plane)" of a sample. In figure 7 a box can be seen, which represents a sample, in which these two descriptions (surface and bedding) are illustrated.

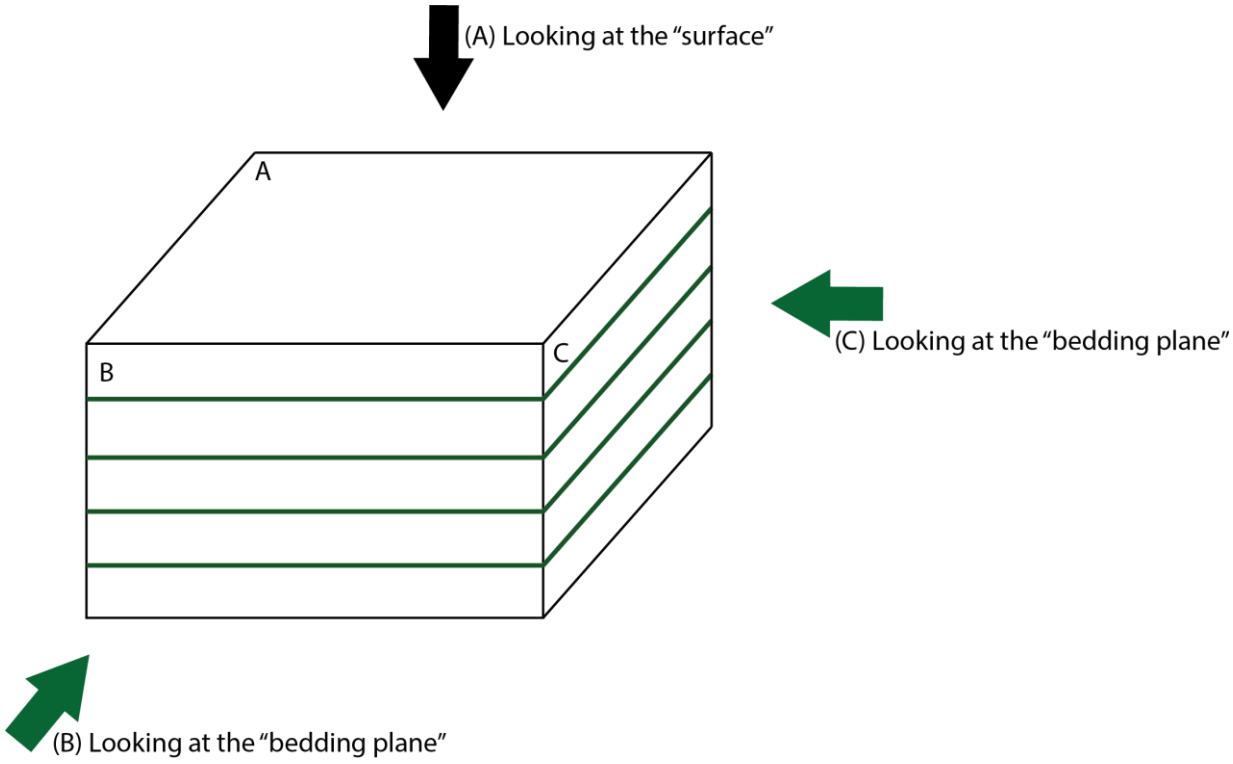

Figure 7. Illustration of the two different descriptions that can be given for a sample. The sample will be either described by 'looking at the surface of a sample', which is resembled in the figure as plane A. Or the sample will be described by "looking at the bedding (plane) of the sample", which is resembled in the figure by both plane B and C.

5.1 Unreacted Gothic shale

5.1.1 Mineralogy and structures

The unreacted Gothic shale sample investigated has a smooth surface (see figure 8a/b), so textures of the minerals present are harder to distinguish, but nonetheless some features are recognizable. The sample contains well developed framboidal structures (see figure 8c/d), which EDX-analyses recognize as pyrite. Pyrite is also seen as non-framboidal structures, namely as subrounded grains (see figure 8c/d). Using ImageJ to scale the pictures and analyze the size of the pyrite minerals, the pyrites ranged in sizes from 0.30–9.50 µm in diameter.

The carbonates present in the sample have more blocky to irregular textures (see figure 8e), and are either dolomite (EDX-spectrum contained the elements Mg, Ca, C and O) or calcite (containing Ca, C and O). The carbonate minerals are a bit larger than the pyrite minerals, reaching diameters of up to approximately 42 µm, and are distributed evenly across the surface without being clustered.

There are also dark grey features in the sample (see figure 8e), which have irregular shapes, ranging from small subrounded textures (ranging in sizes from approximately 0.59-4.63 µm in diameter), to large elongated textures (ranging from approximately 7.8 × 2.33 µm to 70.1 × 4.18 µm). These dark grey, irregular shapes are organic matter, as the EDX-analysis showed a spectrum containing the elements carbon (C) and oxygen (O).

To define the matrix minerals present in the unreacted Gothic shale, an EDX-spectrum was used of a whole area, instead of one point. This spectrum contained elements that suggested that the minerals in the matrix are clay minerals (see figure 8f). Its contents were high in silicon (Si) and O, medium in aluminium (Al), and minor in sodium (Na), magnesium (Mg) and potassium (K).

5.1.2 Porosity

The pores seen in the unreacted Gothic shale are scarce, but present. While some pores are found randomly in the matrix of the sample or even in the organic matter, most of the pores are clustered together with different and larger minerals in between the pores (see figure 8g). A histogram is given in which the amount of pores in the sample is plotted against the surface area of the pores for four different magnifications (see figure 13). The mean pore surface area found in the unreacted shale ranged from 0.041–0.19 μm^2 (see table 2). The reason why the average surface area of a pore ranges, is because it differs per magnification. At a high magnification, smaller pores are more visible than at a low magnification, due to the fact that

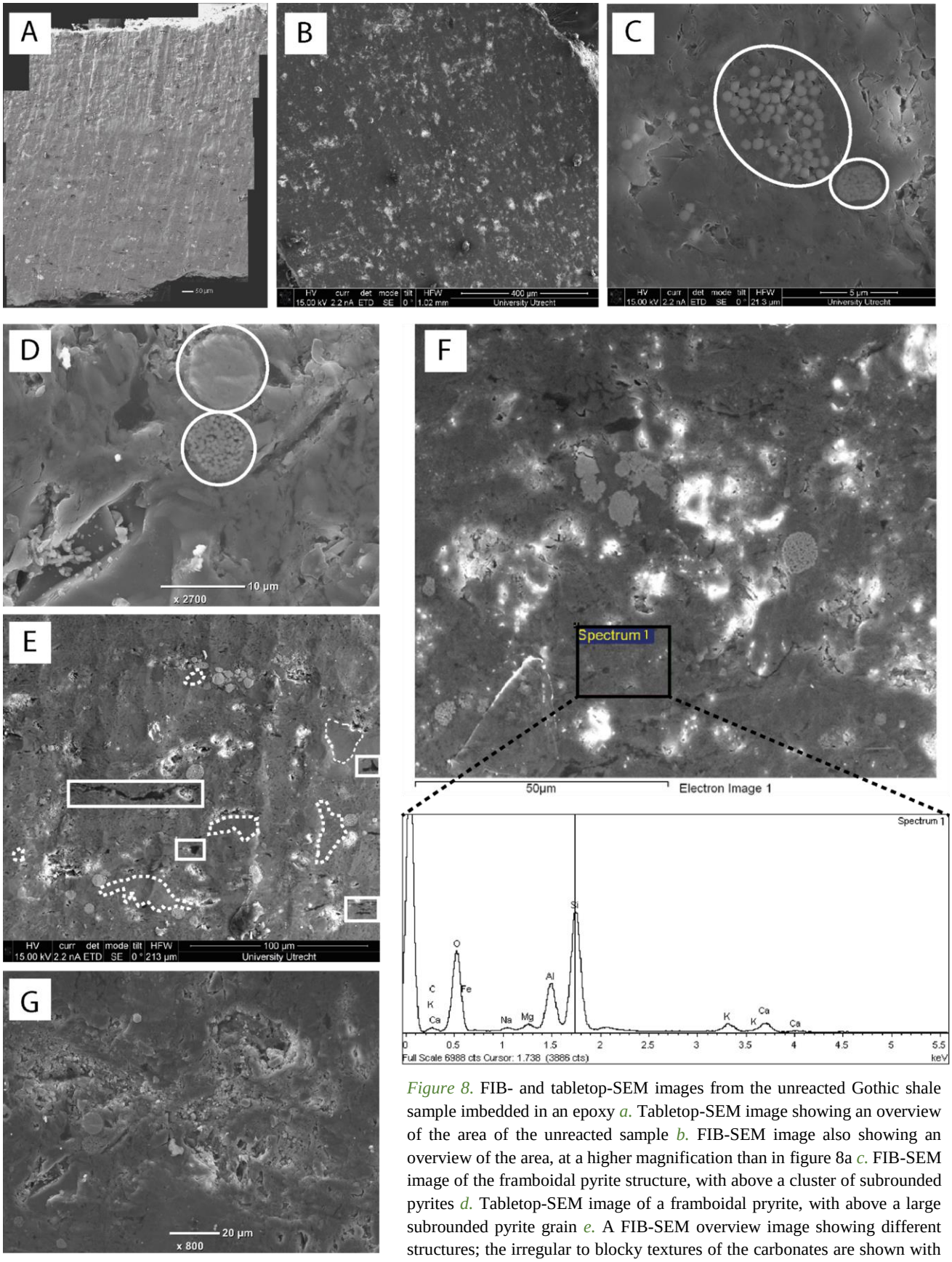

Figure 8. FIB- and tabletop-SEM images from the unreacted Gothic shale sample imbedded in an epoxy *a.* Tabletop-SEM image showing an overview of the area of the unreacted sample *b.* FIB-SEM image also showing an overview of the area, at a higher magnification than in figure 8a *c.* FIB-SEM image of the framboidal pyrite structure, with above a cluster of subrounded pyrites *d.* Tabletop-SEM image of a framboidal pryrite, with above a large subrounded pyrite grain *e.* A FIB-SEM overview image showing different structures; the irregular to blocky textures of the carbonates are shown with a dashed line; the organic matter is shown in rectangular blocks *f.* An element map showing that the matrix contains elements often found in clays *g.* Tabletop-SEM image showing how the pores are mostly clustered together in the unreacted Gothic shale.

the resolution is better. In table 2, the total pore surface area of the unreacted Gothic shale is given for the same four magnifications as in the histograms, along with the number of pores, mean pore surface areas, and the standard deviation.

5.1.3 Mineral precipitation and swelling clays

As the sample has a flat surface, it is impossible to say something about the clays present (if they have swelling features or not). If there was already signs of swelling clays before any reaction took place, this can unfortunately not be detected due to the polished surface of the unreacted Gothic shale.

5.2 Industrial fracking fluid (EHR-001)

5.2.1 Mineralogy and structures

The Gothic shale samples which were experimentally injected with industrial fracking fluid, were put under the tabletop SEM and FIB-SEM as a whole rock, instead of being put into an epoxy and cut to a smooth surface. At the surface, the samples contained a lot of subrounded to blocky mineral grains laying on top of a matrix of flat grains (see figure 9a/b). When looking at the bedding planes of the samples, the subrounded and blocky mineral grains were alternated with platy/sheet-like minerals instead of the flat minerals seen at the surface (figure 9c/d). The flat mineral grains at the surface and the platy/sheet-like minerals in the bedding planes turned out to be the same type of minerals, just at a different angle. The EDX-spectrum showed that these minerals are clays, as the Si, Al and O content were very high, with minor Mg, Fe and K content.

EDX-analysis showed that the blocky grains were often carbonates, both dolomite and calcite, while other smaller subrounded grains were either pyrite or clay particles. The carbonate grains varied a lot in size, with mainly small grains of a few microns, but some grains could reach up to approximately 20–30 µm in diameter. The well-developed framboidal pyrite structures seen in the unreacted sample were not visible in these samples.

5.2.2 Porosity

The pores seen at the surface of the bedding planes differ from the pores seen in the bedding planes. The pores on the surface are, in general, much less frequent than in the bedding (see figure 9e/f). The bedding also contains cracks, which causes a large area of porosity (see figure 9g/h). Cracks are not or hardly visible on the surface of the EHR-001 sample.

The mean pore surface area differs per magnification. As stated before, this is due to the fact that at a higher magnification the resolution is better, making it easier to detect smaller pores, than at a low magnification. Another thing that should be mentioned is that a lower magnification also takes cracks into account as the surface area observed is larger than that of a high magnification. These cracks increase the pore surface a lot, but also result in a higher number for the standard deviation. This can be illustrated in an example; At a magnification of x300, the total pore surface area of the image is 2001.91 μm^2, while the mean pore surface area is 1.045 μm^2 with a standard deviation (σ) of 6.621 for a measured number (n) of 1915 pores; these numbers change for a magnification of x850, in which the total pore surface area is 468.8 μm^2, the mean pore surface area is 0.325 μm^2 with σ = 1.257 and n = 1443. The standard deviation lowers significantly with a higher magnification.

In table 2 the mean pore surface area is given for the other magnifications, along with the total pore surface area, standard deviation and amount of pores measured. In figure 13 the porosity of the EHR-001 samples is plotted in a frequency vs. pore surface area histogram for the same four magnifications. This is done by taking the porosity of the whole rock, instead of describing the porosity of the surface and bedding separately. The trend seen in the histograms of figure 13, shows that the frequency decreases when the pore size increases.

5.2.3 Mineral precipitation and swelling clays

The samples that reacted with industrial fracking fluid do not show any clear sign of swelling clays, as the clay sheets are seen as very thin layers/sheets (see figure 9d). The samples do have a large amount of small grains, which are precipitated minerals due to the reaction of the Gothic shale with the fracking fluid. These are precipitated grains as the element distribution in the EDX-spectrum have changed slightly from the unreacted Gothic shale sample. When doing an EDX-analysis on the subrounded grains, a large amount turned out to be clay minerals. These grains were recognized as clays because the amount of Si and Al were high in content, and it contained a medium to minor amount of the elements Fe, K, Ca and Mg. The blocky to irregular shaped precipitated grains, are carbonate minerals. The carbonate minerals are recognized as dolomite, as the EDX-spectrum contains Mg as element next to Ca, C and O. The precipitated dolomite is related to the reaction of the fracking fluid with the unreacted Gothic shale, and is deposited evenly over the exterior of the fracking fluid samples.

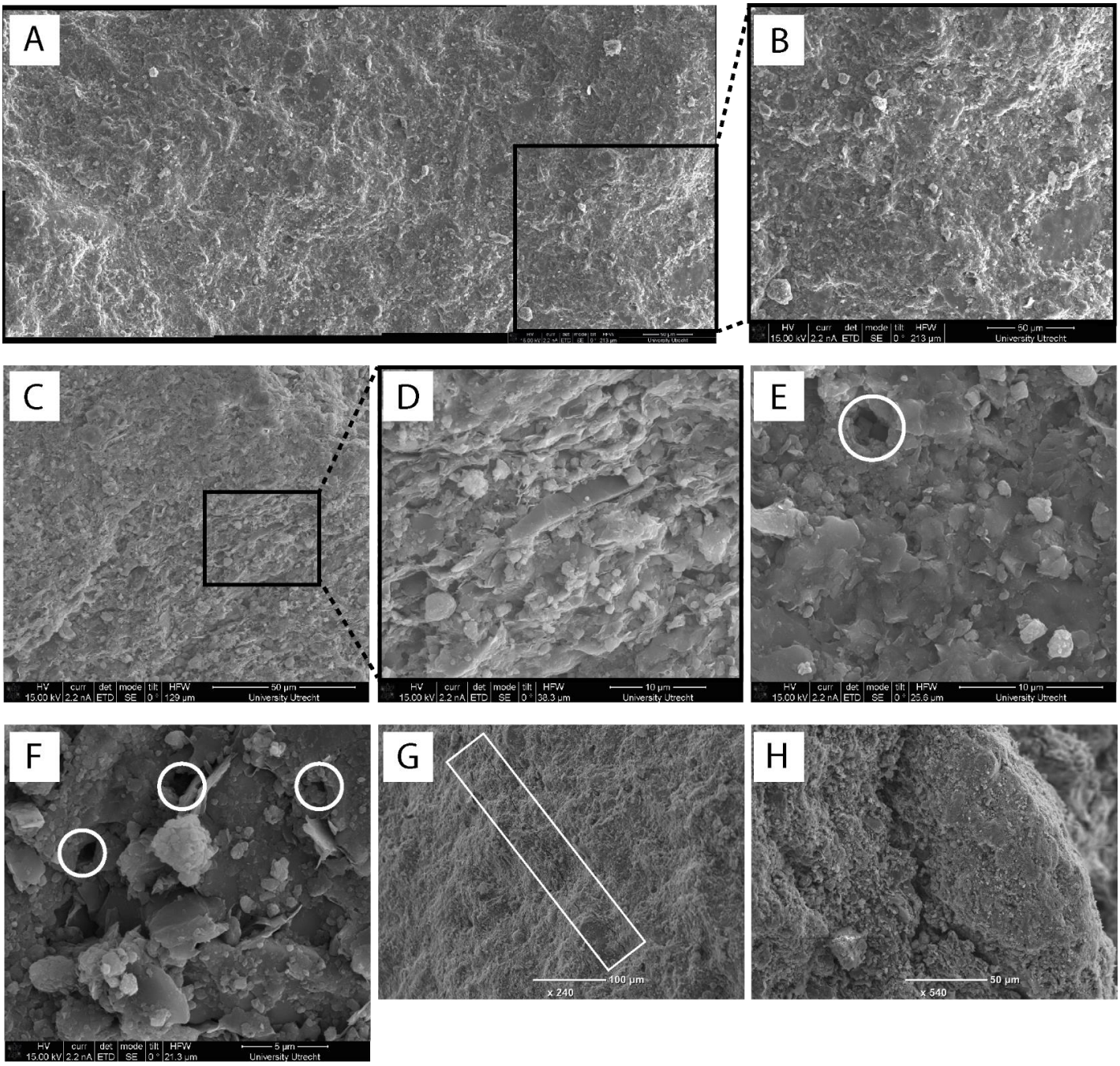

Figure 9. FIB- and tabletop-SEM images of the samples reacted with industrial fracking fluid (EHR-001 samples) *a.* FIB-SEM image showing a large overview of the surface area, the black box is the part that contains figure 9b *b.* FIB-SEM image zooming in on the surface overview of figure 9a, showing the blocky/irregular carbonates on top of flat clay grains *c.* FIB-SEM image showing an overview of the bedding planes area, with the black box as figure 9d *d.* FIB-SEM image zooming in on the platy/sheet structure of the clays seen in the bedding planes *e.* A FIB-SEM image showing a pore at the surface of the EHR-001 *f.* A FIB-SEM image showing pores in the bedding planes of the EHR-001 samples; the magnification is higher than the image of figure 9e, but nevertheless shows a higher amount of pores in the bedding plane than the amount of pores at the surface *g.* Tabletop-SEM image of the bedding plane showing a very long crack in the white rectangle, at a magnification of x240 *h.* Tabletop-SEM image of the bedding plane showing a very large crack, at a magnification of x540

5.3 CO_2-fluid (EPA-1)

5.3.1 Mineralogy and structures

At the surface of the samples that have reacted with CO_2-fluid, the samples contained a lot of subrounded to blocky mineral grains laying on top a matrix of flat minerals (see figure 10a). These flat minerals are shown to be clay minerals by EDX analysis as the Si, Al and O content were very high. The subrounded to blocky grains are carbonate minerals (both dolomite and calcite), containing the elements Ca, C and O, with dolomite also containing Mg. The carbonate minerals are not large in size and usually are only a few microns (up to 10 µm across) or even smaller, but there are a few exceptions where the carbonates can reach up to 25–40 µm in diameter. The bigger grains are distributed evenly on the surface among the smaller grains and do not cluster together. At the bedding planes the same features are seen, only the flat clay minerals seen at the surface, are now seen as clay sheets (figure 10b).

Pyrite is also present in the samples, but do not have the framboidal structures seen in the unreacted Gothic shale. The pyrites are often only recognizable with the use of element mapping where there are strong spots containing both the elements iron (Fe) and sulfur (S) (figure 11). The pyrites in these sample are only rarely seen as distinguishable minerals.

5.3.2 Porosity

The porosity of the samples have increased a lot compared with the unreacted Gothic sample (see table 2). The pores seen at the surfaces, are large in number, but small in size (e.g. at a magnification x600, n = 2711, mean pore surface area = 0.491µm^2, σ = 1.783; see table 2 for different magnifications). In the bedding planes the pores seem to be a bit larger and more present than at the surface of the bedding planes (see figure 10c/d). The mean pore surface area of the surface and bedding planes together varies from 0.539–1.341 µm^2 depending on the magnification used (high magnification and low magnification, respectively). In table 2 the total pore surface area is given, along with the mean pore surface area, standard deviation and number of pores, for the four magnifications. The distribution of pores can also be seen in figure 13, in which the frequency of the pores is plotted against the pore surface area. Figure 13 shows the four magnifications described in table 2.

An important contributor for the pore surface area are the cracks found in the samples. The most cracks are seen in the bedding planes (see figure 10e). At the surface of the bedding planes cracks are also visible, but they are much less frequent and can only be found near the edges of the samples (see figure 10f). Another feature that increases the porosity in the samples are the

dissolution features, seen as holes/pores in the exterior, with edges that are irregularly shaped (see figure 10g).

5.3.3 Mineral precipitation and swelling clays

The EPA-1 samples show thicker clay sheets at some places, which resembles the swelling of clays (see figure 10h). The feature of swelling clays is only recognized at a high magnification, when looking for it specifically. Swelling clays are only found when looking at the bedding planes, as here the clays are seen as sheets instead of flat grains like at the surface.

Another feature already mentioned is the large amount of very small grains on the exterior of both the surface of the bedding planes and the exterior of the bedding planes themselves. These small grains that reach only up to a few microns in size, are often subrounded precipitated clays, analyzed with EDX (spectrum shows high Si, O and Al content). But also precipitated blocky to irregular carbonate grains are found on the exterior. These carbonate minerals are distributed evenly across the exterior and contain elements such as Fe and Mg alongside the carbonate elements. The precipitation minerals are formed due to the reaction of the CO_2-fluid with the Gothic shale.

5.3.4 3D-slab

The shale sample that has reacted with CO_2-fluid, was the only sample of which a 3D-slab was made under the FIB-SEM. The cutting process took place on a crack visible in the bedding plane of one of the EPA-1 samples (see figure 11i). This is done to find out if the crack extends to the interior of the sample, or if the crack is only visible near the exterior of the sample. Another reason to cut at a place that contains a crack, is to find out if the same happens with the pores; are the pores only found at the exterior where the CO_2-fluid reacted with the sample, or does it also flow through the cracks and generates porosity in the interior?

The 3D-slab that was produced from the cutting process can be seen in figure 11j, with a close up look of that same slab in figure 11k. In the 3D-slab, pores can be seen near the surface, but also near the crack. In figure 11L, the same figure of 10k is combined with colour-coding; the area which represents the exterior of the bedding plane, is coloured black; the area of the crack contains dashed black lines; the area containing pores in the 3D-slab is coloured green; and the area in the 3D-slab without pores is coloured brown.

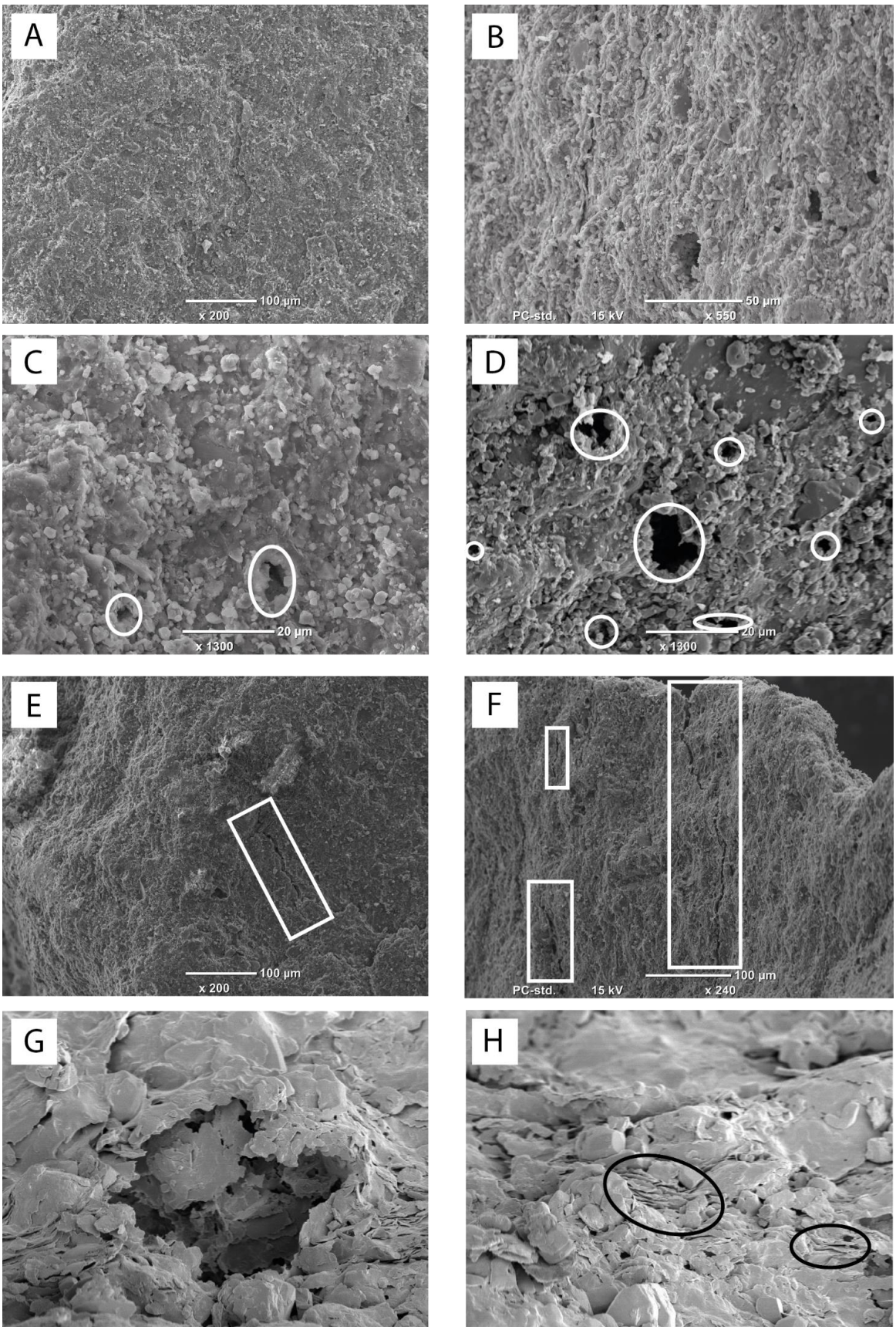
A
100 µm
x 200
B
PC-std. 15 kV
50 µm
x 550
C
20 µm
x 1300
D
20 µm
x 1300
E
100 µm
x 200
F
PC-std. 15 kV
100 µm
x 240
G
H

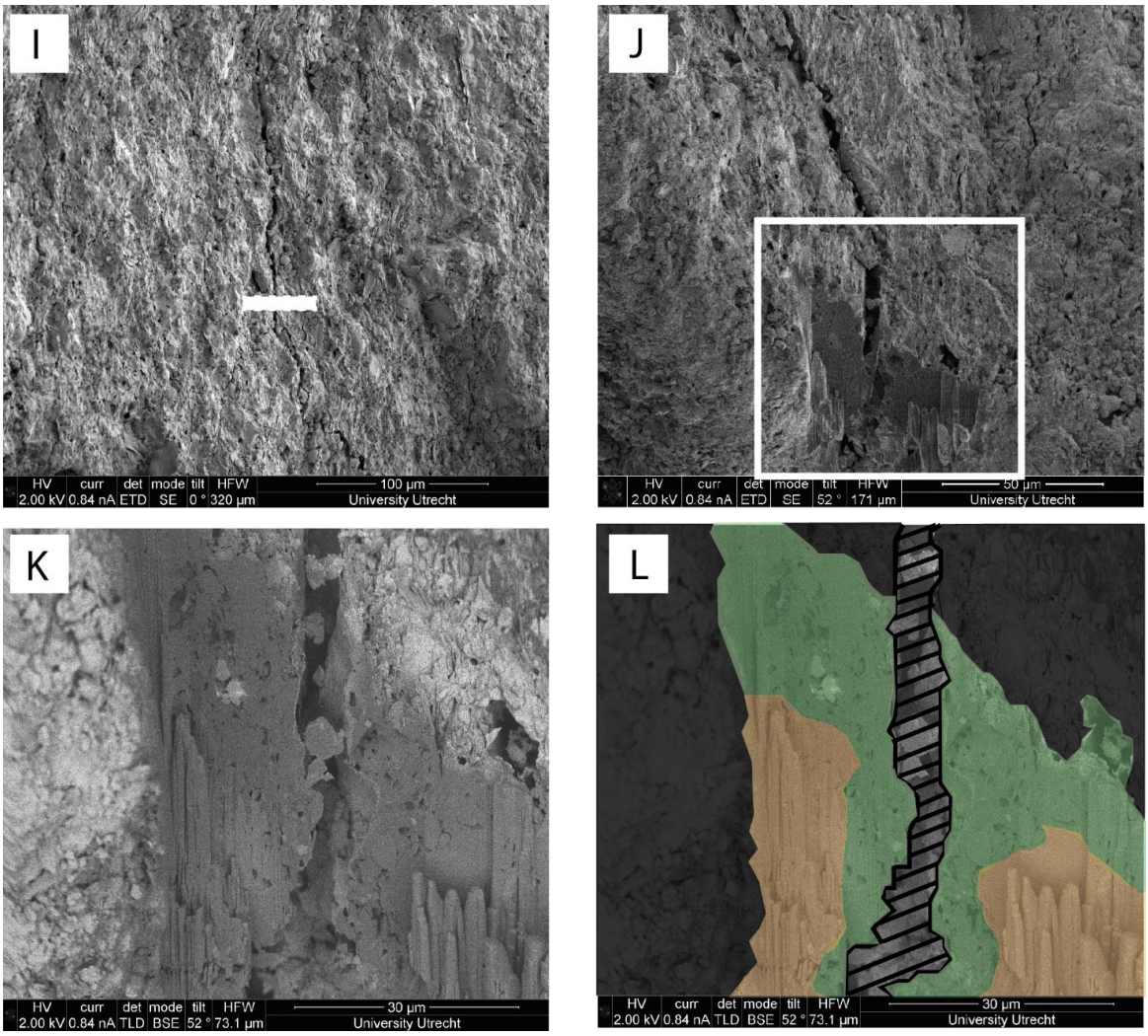

Figure 10. FIB- and tabletop-SEM images of the samples reacted with CO_2-fluid (EPA-1 samples) *a.* Tabletop-SEM image showing an overview of the surface area, with blocky/irregular carbonates on top of flat clay grains *b.* Tabletop-SEM overview of the beddings planes area, showing the sheet-like structure of the clays *c.* Tabletop-SEM image showing the pores seen at the surface of the EPA-1 samples *d.* Tabletop-SEM image showing the pores seen in the bedding planes of the EPA-1 samples *e.* A tabletop-SEM image, which shows a crack near the edge, at the surface *f.* Tabletop-SEM image showing large cracks and smaller crack found in the bedding planes of the EPA-1 samples *g.* FIB-SEM image of the dissolution textures sometimes seen in the samples *h.* FIB-SEM image showing how the clays seem to swell when in contact with the CO_2-fluid *i.* FIB-SEM image showing the location (white rectangle) where the ion beam cutting took place *j.* FIB-SEM image of the 3D-slab that has been cut out *k.* FIB-SEM image zooming in on the 3D-slab seen in figure 11j *l.* FIB-SEM image of the exact same figure as 10k, but this time showing colour-coding; the area which represents the exterior of the bedding plane, is coloured black; the area of the crack contains dashed black lines; the area containing pores in the 3D-slab is coloured green; and the area in the 3D-slab without pores is coloured brown.

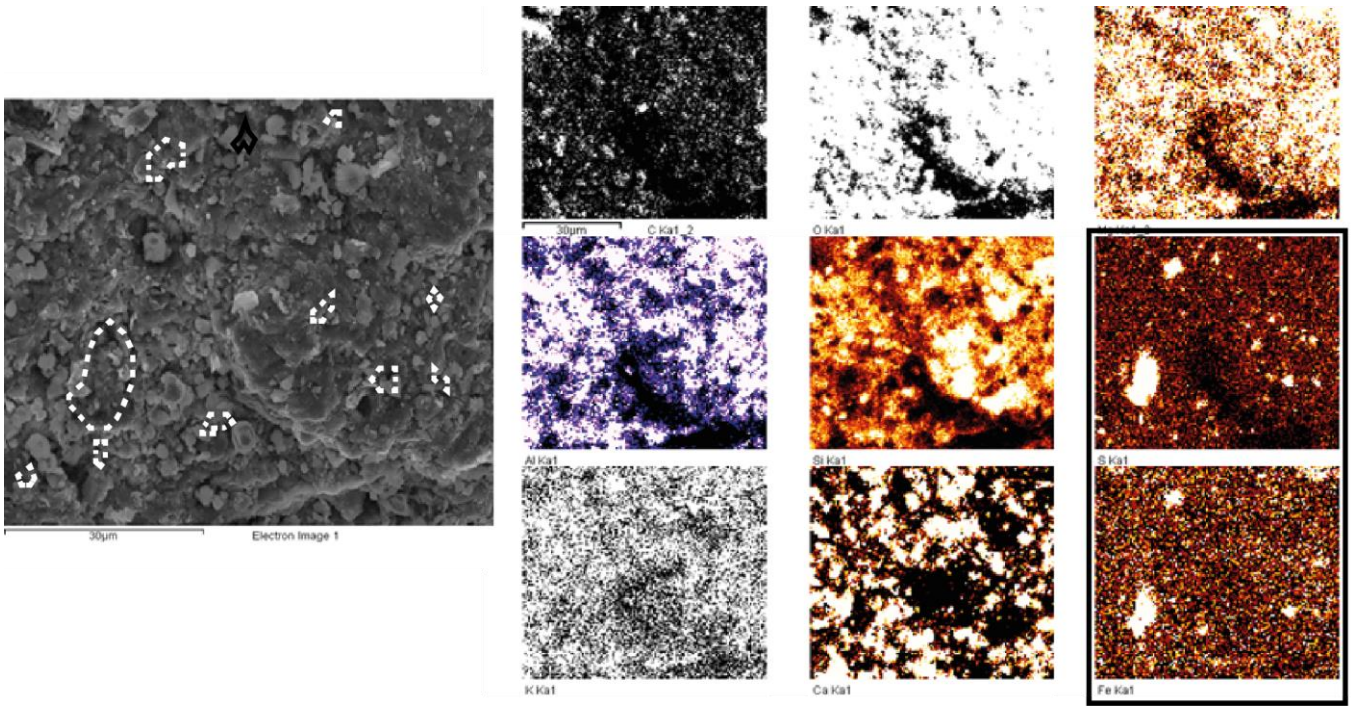

Figure 11. Element mapping of the sample reacted with CO_2-fluid (EPA-1), conducted on the FIB-SEM, which shows that the pyrite found in the samples do not always have distinguishable mineral grains. The two element maps in the black box, represent sulfur and iron (above and below, respectively). These two elements are the components of pyrite (FeS_2). When looking at the electron image to the left, the areas are encircled with a white dashed line where the sulfur and iron elements are concentrated. These white lines do not represent a mineral grain, giving the idea that pyrite is spread out over the EPA-1 sample.

5.4 Brine (EPA-2)

5.4.1 Mineralogy and structures

The exterior of the EPA-2 samples is much more chaotic than those of the other type of samples investigated. Many more small subrounded minerals can be seen on both the exterior of the surface as well as on the bedding planes. At the surface not a lot of the flat minerals, seen in both EHR-001 and EPA-1, are visible due to the filling up of the subrounded grains (see figure 12a). In the bedding planes the flat minerals are distinguishable as sheets (see figure 12b). EDX-analysis showed that the sheets seen in the bedding planes and the flat minerals at the surface, are clay minerals. This is due to the high content of Si, O and Al, with the medium to minor content of the elements Fe, K, Mg and Ca. The frequent, subrounded to blocky grains appeared to be both clay minerals as well as carbonate minerals (both dolomite and calcite). The clay minerals were often found to be the subrounded grains, while the carbonates were blocky to irregular in shape. The size of most of the carbonates were only a few microns large, but there were some exceptions where the carbonates reached a size of approximately 15–20 µm across.

An element map showed that the samples also contained pyrite minerals, which were not always clearly recognized as a separate mineral.

The framboidal pyrite structure seen in the unreacted Gothic shale was also scarcely seen in the EPA-2 samples (see figure 12c). A new structure that has not been seen in any of the other type of sample is a sort of banding structure in the bedding planes, which seem to alternate between bands with of a lot pores and bands of hardly any pores (see figure 12d). These bands also vary in relief, in which the bands with a lot of pores are lower in relief than the bands with hardly any pores. As in the EPA-1 samples, dissolution features are also seen in these samples (see figure 12e/f), but have much more irregular surfaces than seen in the EPA-2 samples. The irregular textures of the holes/pores seen on the exterior show that a reaction of dissolution must have occurred when the brine came into contact with the unreacted Gothic shale.

5.4.2 Porosity

The porosity of the samples is less than in the EHR-001 and EPA-1 samples, but nonetheless it has increased compared with the unreacted Gothic sample (see table 2 for actual numbers showing the increase of porosity compared to the unreacted sample). The pores at the surface and the pores at the bedding planes look the same, as they both have approximately the same size, shape and amount. Therefore difference between these pores is hard to distinguish (see figure 12g/h). The average pore surface area of the sample varies from 0.164–0.69 μm^2 depending on the magnification used (high magnification and low magnification, respectively). Table 2 gives the average of the total pore surface area for the EPA-2 samples at four different magnifications. Figure 13 shows the same four magnifications used for table 2, in which the distribution of the pores can be seen versus the pore surface area. Less cracks are found in the brine samples compared to the CO_2 samples, but they are still an important contributor for the pore surface area (see figure 12i/j). In figure 12i, it can be seen that the bedding planes clearly do have larger cracks when comparing it to the cracks at the surface, as shown in figure 12j.

5.4.3 Mineral precipitation and swelling clays

The samples that have been put into brine-solution sometimes show clay sheets that have swelled due to reaction with the brine. For the brine reacted samples, the sides parallel to the bedding planes were used to detect the presence of swelling clays (figure 12k). The swelling of clays is less present in these samples than in the carbonated (EPA-1) samples and therefore harder to find.

The samples also contain precipitated minerals as there are a lot of small grains on the exterior of the samples, most of them with an irregular shape. EDX-analysis showed that these minerals are mostly clays, just like the EHR-001 and EPA-1 samples, but also some carbonate minerals are precipitated. The chaotic structure present in the EPA-2 samples is due to the large amount of these precipitated carbonate and clay minerals, which is the most predominant feature in these samples compared to the other fluids (industrial fracking fluid and CO_2-fluid).

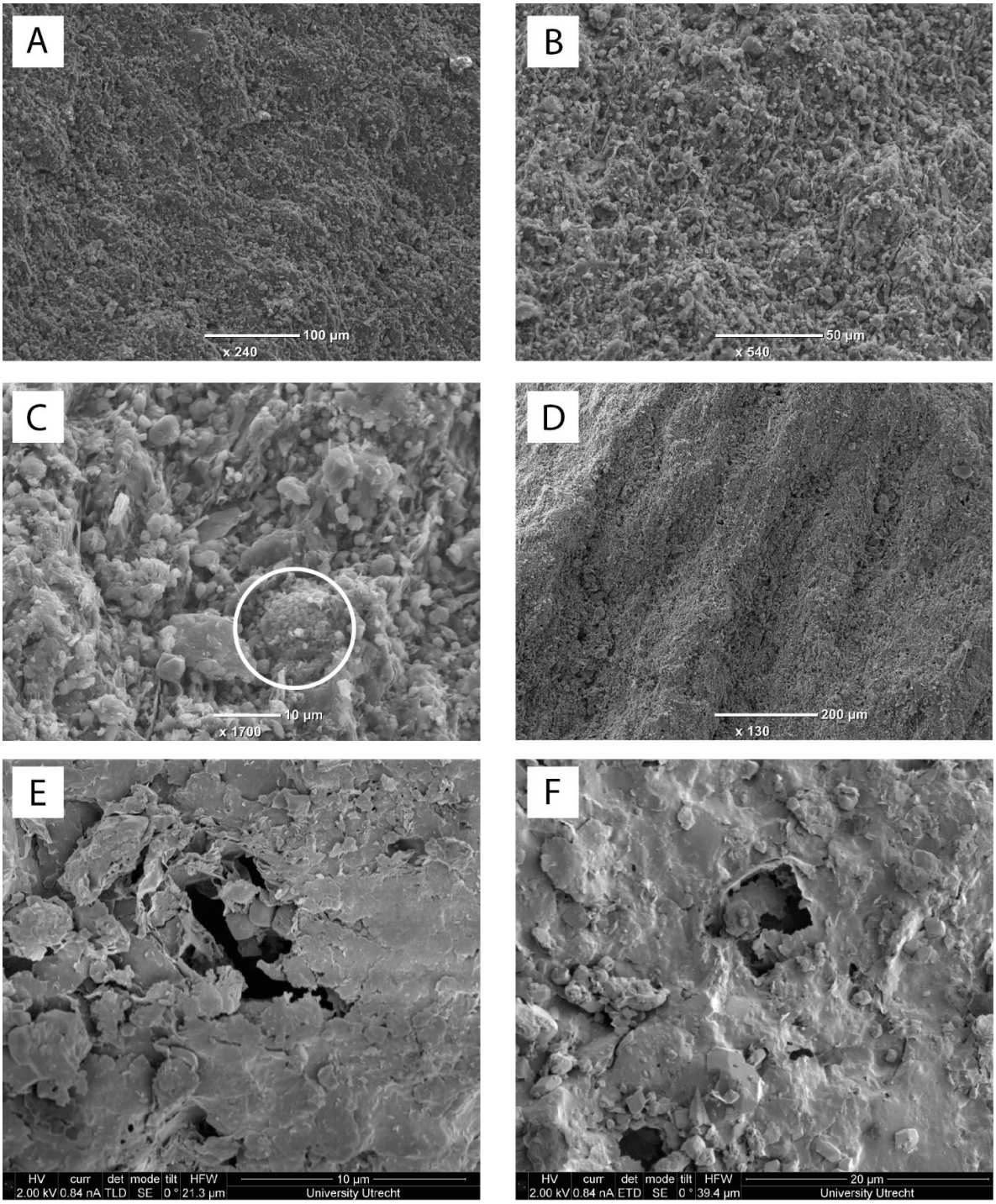

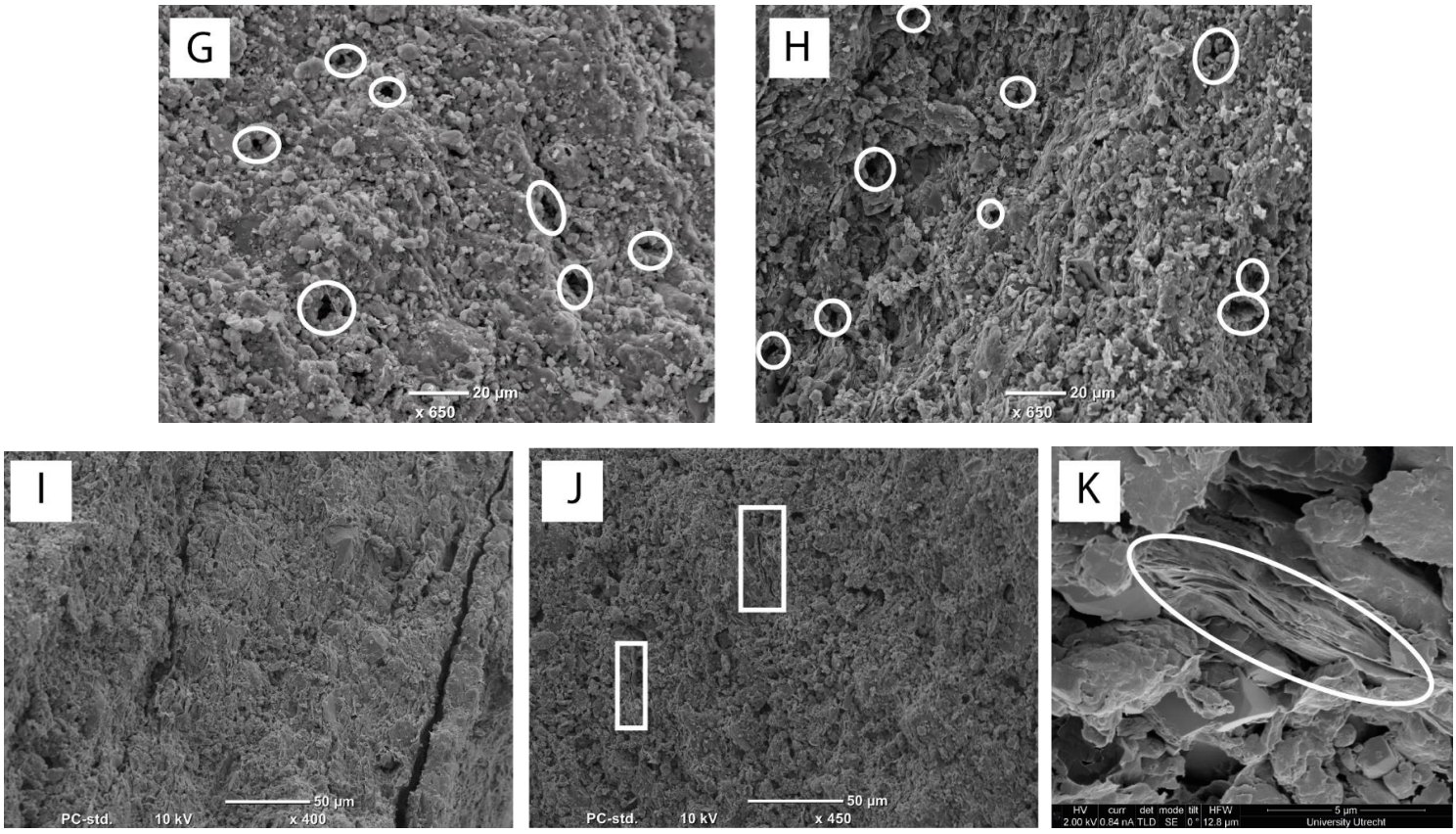

Figure 12. FIB- and tabletop-SEM images of the samples reacted with brine (EPA-2 samples) *a.* Tabletop-SEM image showing an overview of the chaotic surface area *b.* Tabletop-SEM overview of the beddings planes area, showing the sheet-like structure of the clays *c.* Tabletop-SEM image showing a framboidal pyrite structure *d.* Tabletop-SEM image showing the banding found in the bedding planes with areas of much porosity alternating each other with areas of little porosity. It also shows alternation in relief, where the areas with more pores a lower in relief than the area with less pores *e/f.* Two FIB-SEM images illustrating the dissolution structures found in the EPA-2 samples *g/h.* Tabletop-SEM image of the pores found on the surface and bedding planes, respectively. They contain approximately the same size and amount of pores *i/j.* Tabletop-SEM images of the cracks found in the bedding planes and at the surface, respectively. The bedding planes clearly do have larger cracks than at the surface *k.* FIB-SEM image showing how the clays seem to swell when in contact with the brine.

Table 2. Total pure surface area (SA, µm^2), number of pores (n), standard deviation (σ) and the mean pore surface area (mean, µm^2) of the four different samples, measured at four different magnifications (x300, x600, x850 and x1500).

Magn.	Unreacted				CO_2-fluid (EPA-1)				Brine (EPA-2)				FF (EHR-001)			
	SA	n	σ	mean	SA	n	σ	mean	SA	n	σ	mean	SA	n	σ	mean
x300	36.39	192	0.247	0.19	1861.65	1933	6.817	1.341	561.34	814	4.147	0.69	2001.91	1915	6.621	1.045
x600	×				1581.4	2711	1.783	0.491	643.45	1013	0.294	0.355	1252	2318	2.136	0.456
x850	11.11	121	0.218	0.095	388.3	1594	0.258	0.39	131.73	2374	1.047	0.13	468.8	1443	1.257	0.325
x1500	3.102	64	0.241	0.046	146.14	442	1.030	0.54	108.73	869	0.668	0.165	×			

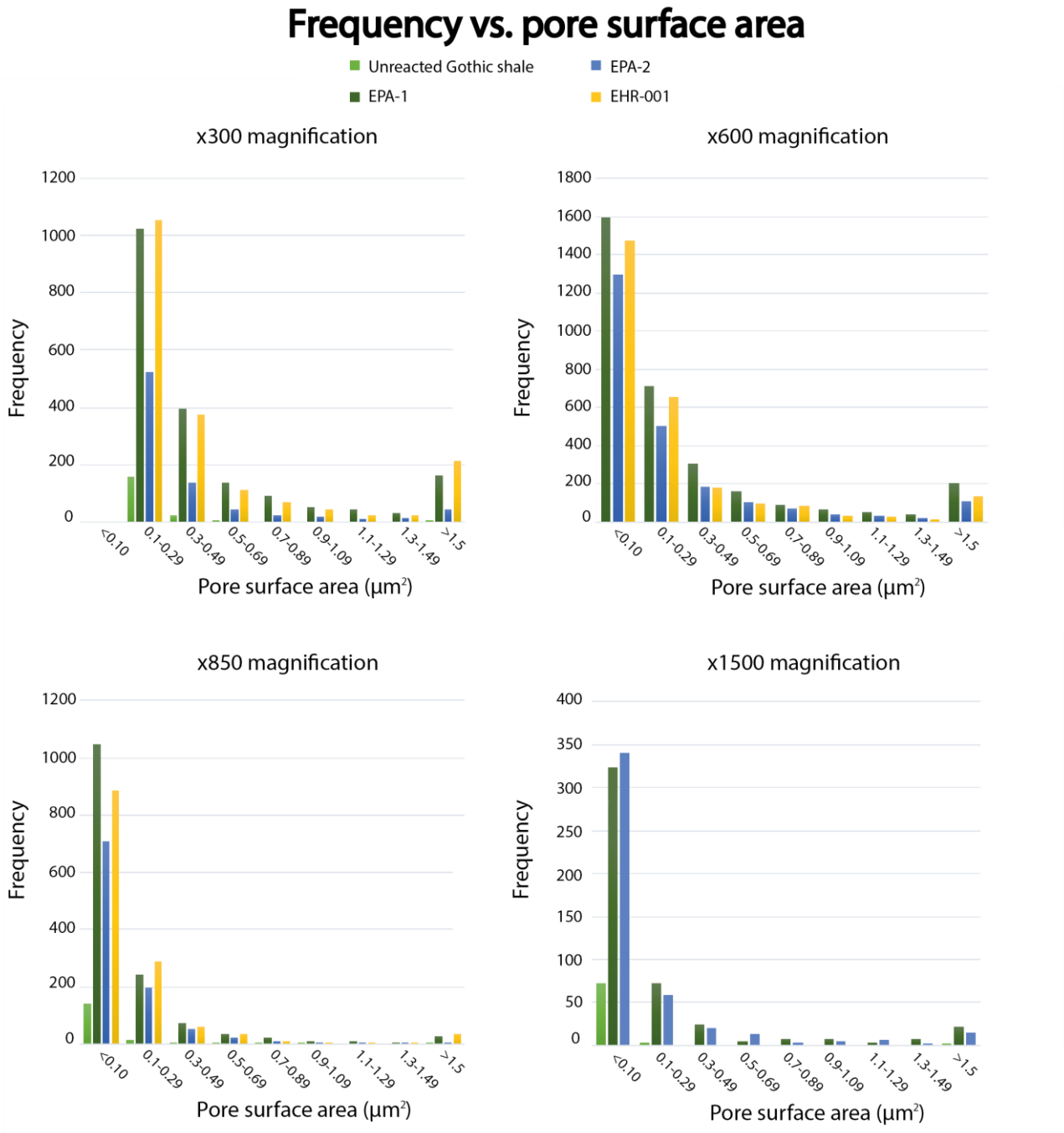

Figure 13. Diagrams giving the distribution of the pores. The frequency of the pores is plotted against the pore surface area. This is done for four magnifications: x300, x600, x850 and x1500

6. DISCUSSION

In this part of the paper the results will be discussed in four different sections. First the samples will be compared to one another, to establish the differences in the samples. A possible explanation for these differences will then be provided, which will lead to a comparison and discussion using the theory overview (given in chapter 3) and the results of this study. At the end of this chapter, there is a short section that will discuss the problems and uncertainties encountered during this study.

6.1 Comparing the samples to one another

6.1.1 Dissolution features

Recognizing pores in the matrix from pores formed due to the dissolution of certain minerals was established by looking at the boundary of the pores. Most pores seen in this study are irregular in shape, but while the boundaries of the matrix pores most often have smoother textures, the pores formed during dissolution have irregular boundaries (see figure 14). The clearest dissolution textures were present in the CO_2-fluid (EPA-1) and brine (EPA-2) reacted samples. It would be suspected that the industrial fracking fluid also has dissolution features as the fluid reacts with the unreacted shale, but these were not as evident as in the CO_2-fluid and brine reacted samples. An indication that dissolution took place in the fracking fluid samples, was seen in the irregular and small minerals that precipitated onto the surface of the sample. However, it could not be identified in the pore boundaries as the fracking fluid had relatively smooth pore boundaries.

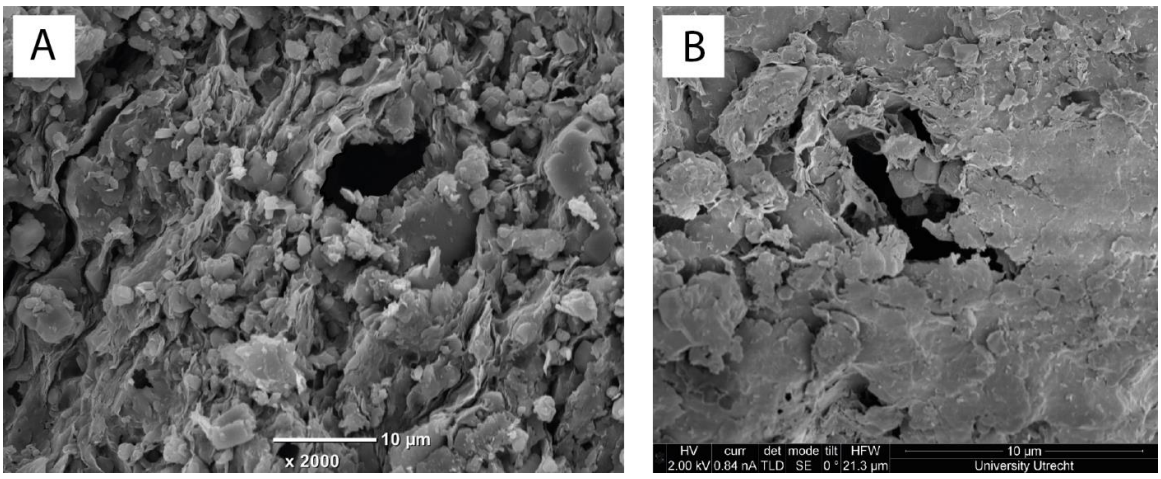

Figure 14. SEM images showing the difference between (a) matrix pores (tabletop-SEM image) and (b) dissolution pores (FIB-SEM image)

The brine reacted samples have dissolution textures that are even more irregular compared to those seen in the CO_2-fluid. Next to this, the dissolution textures in the brine samples are also much easier to find when looking at the samples under the tabletop- and FIB-SEM, as they are more present in these samples than in the CO_2 samples. Another feature that can be seen near pores formed due to dissolution, is that near or even in these pores a lot of smaller grains are found.

6.1.2 Cracks

Cracks are important features to find in the samples, as they are big contributors to the total porosity and are useful to gain more permeability in the shale rock. They are also the reason why the standard deviation in table 2 is sometimes much higher than expected when looking at the pores of the samples (described in 6.1.3).

The unreacted Gothic shale does not have any cracks on its polished surface. When looking at the surface of the other three samples, perpendicular to the bedding plane, it turns out that cracks are hard to find on the surface of each sample type, especially on the surface of the brine and fracking fluid reacted samples (see figure 15). Cracks on the surface of the CO_2-fluid reacted sample are easier to distinguish, as they are the clearest and widest cracks found on the surface of the samples (see figure 15b). As already stated in the results section, the cracks on the surface of the CO_2-fluid samples, are found near the edges of the sample.

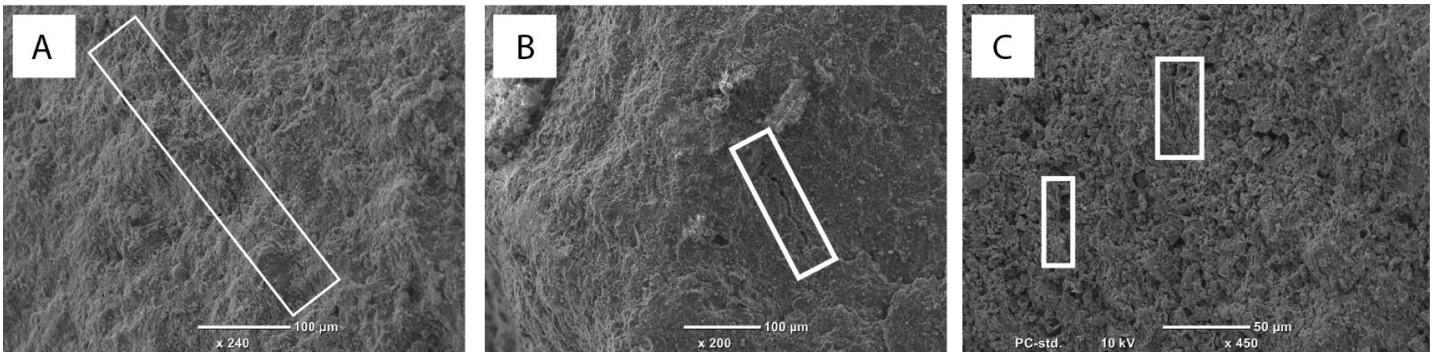

Figure 15. Tabletop-SEM images of the cracks found on the surface of (a) the fracking fluid (EHR-001) samples (b) the CO_2-fluid (EPA-1) sample and (c) the brine reacted (EPA-2) sample. Note the scale bar for comparison. The clearest and widest crack is that of the CO_2-fluid sample, which is imaged at the lowest magnification (x200). The cracks visible in the brine reacted sample are very small in comparison, as they are images at higher magnification (x450)

In the bedding planes of the three fluid-reacted samples the cracks found are different than those of the cracks on the surface. The cracks are much more present in the bedding planes, but while the brine reacted sample contains the least cracks, the CO_2 fluid and fracking fluid contain the most with roughly the same amount. The size of the cracks found in the bedding planes are

approximately the same for the three reacted samples. Another noteworthy feature is that all the cracks found in the bedding planes are parallel to the bedding planes. The only difference between them, is the frequency in which they are found.

6.1.3 Pores

The pores in each sample have already been listed in table 2. The least pores were present in the unreacted Gothic shale. Compared to the unreacted sample, all the samples show an increase in porosity due to the reaction with the fluid involved. In the unreacted shale the pores are most often found clustered together, while in the CO_2-fluid and fracking fluid samples the pores are distributed evenly across the exterior of both the surface of the sample as well as the bedding planes of the sample. This is different for the brine reacted sample, as these samples show an even distribution on the exterior of the surface, but show a sort of banding structure on the exterior of the bedding planes.

The CO_2-fluid and fracking fluid contain pores that are most alike one another. The two type of samples have approximately the same amount of pores, mean pore surface area, standard deviation, but also roughly the same total pore surface area (see table 2). The CO_2-fluid and fracking fluid samples compete with each other in having the largest pore surface area, depending on the magnification used (see table 2). The brine samples also have an increase in porosity compared to the unreacted Gothic shale, but much lower than the CO_2- and fracking fluid samples. In table 2 however, it can be observed that the brine samples do have a very high amount of pores, sometimes even higher than that of the CO_2 and fracking fluid samples.

As figure 13 shows, all the samples contain the most pores which are small in size (pore surface area < 0.10 μm^2). The frequency of the pores decreases with increasing pore surface area, with only a few exceptions. These exceptions are most likely due to cracks in the image which have also been analyzed as a pore. Cracks often have a larger surface area than the pores, and therefore can cause the standard deviation seen in table 2 to be much larger than expected. Another thing to keep in mind is that the higher the magnification, the lower the standard deviation gets. This is because at a low magnification the size of the total surface area seen in the image is greater than that of a high magnification, which can therefore include much more cracks seen at the surface, causing the higher standard deviation. The brine samples and the unreacted sample have the lowest standard deviation. This also explains why the brine samples can have such a high number of pores, but a lower total surface area than the CO_2- and fracking fluid samples. The mean pore surface area of the brine samples is much lower than the mean

pore surface area of the other two samples, while the standard deviation is also quite small in comparison with the other two samples.

6.1.4 Precipitation

Precipitation is a feature you would expect to find when a reaction took place. The unreacted Gothic shale sample is taken as representative for the starting material as it is found in the subsurface. This means that there are no precipitated minerals on the surface of the unreacted Gothic shale. To distinguish the precipitated minerals found in the other three sample from the matrix minerals (analyzed in the unreacted sample), EDX-analysis was used to find out if the minerals involved showed a different element distribution from the matrix minerals. If so, these minerals were recognized as precipitation minerals, formed due to the reaction of the Gothic shale with the fluid involved. The most precipitated minerals found in the brine, CO_2- and fracking fluid samples are clay minerals. Carbonate precipitated minerals are also found, but much less in frequency than the clay minerals. In the three reacted samples the precipitation is spread out evenly across the exterior and not clustered in specific areas.

The brine reacted samples have the most precipitated minerals of all the type of samples. The exterior of the brine samples is full of small subrounded precipitated clay minerals, with a few exceptions in which the minerals are blockier to irregular in shape and represent carbonate precipitation. This causes the exterior of the brine samples to look much more chaotic than all the other samples. The carbonate precipitation is also present in the CO_2-fluid and fracking fluid samples, with the least content (or least found during EDX-analysis) in the fracking fluid samples. Clay precipitation is also found in these two samples, but does not cover the whole exterior as it does in the brine samples.

6.1.5 Swelling clays

In the theory overview (chapter 3) it has been explained how swelling clays can occur in shales due to interaction with water and CO_2-fluid. In this study signs of swelling clays have also been observed under the microscope (mainly under the FIB-SEM, due to its high resolution). Unfortunately it cannot be said if the unreacted Gothic shale already contained swelling clays, due to its polished surface. For this reason it is assumed that the unreacted Gothic shale has no swelling clays, and that the swelling seen in the other samples, must have occurred due to the reaction of the fluid involved, with the unreacted shale.

In the industrial fracking fluid samples no signs of swelling clays have been found. This could be due to the fact that the EHR-001 samples have mostly been studied under the tabletop-

SEM instead of the FIB-SEM. The latter has a higher resolution, making it easier to detect swelling clays. But nonetheless it is quite logical to not find any swelling clays in these samples as fracking fluid contains a lot of chemicals, including clay stabilizers *(Mohajan, 2012)* which prevent the clay from swelling and migrating.

Both the CO_2-fluid samples as the brine samples show swelling clays. The swelled up clays are not evenly distributed, nor are they clustered, but they seem to be randomly distributed in both the CO_2-fluid and brine samples. To find these swelling clays, you must really look for them, as it is not a very clear characteristic to observe; the clay sheets that have swelled just look a bit thicker than the clay sheets that have not swelled. So to observe the swelling of clays, you must look at the bedding planes in which clear clay sheets are visible and search for thickness differences.

6.1.6 Banding textures

The samples that have reacted with brine, are the only type of sample that shows a banding structure in which bands of pores alternate each other with bands with hardly/no pores. This alternation is highlighted with a difference in relief, in which the bands with a lot of pores are lower in relief than the bands with hardly/no pores. As the other type of samples in this study, do not show this characteristic, the banding textures cannot be compared to the other samples.

6.1.7 3D-slab

In the 3D-slab of the CO2-fluid reacted sample (seen in figure 10k/l), the pores are only found near the surface or near the crack seen in the 3D-slab. This suggests that pores are only generated near the places where the CO2-fluid has access to (reacting with the sample), and that the interior of the sample most likely resembles the unreacted Gothic shale. This is not necessarily a bad thing for the gas industry, as the difference in the samples used for this study and the shales used for gas production, is the following: the samples used here are put into a solution instead of being fracked at high pressure. When fracking at high pressure the shale rock breaks, resulting in cracks that can penetrate into the interior of the rock, making it easier for the fluid to flow to the interior. The samples used here are only put into a solution and not fracked. The fluid involved can therefore only react with the exterior of the sample, and with the possible cracks formed during the reaction with the exterior.

6.1.8 Summarizing the characteristics

All the above characteristics and comparisons have been summarized into table 3, to get a better and simplified overview.

Table 3. Comparing the different characteristics found in the samples to one another

Characteristics	Unreacted	EPA-1	EPA-2	EHR-001
Dissolution features	-	+	++	+/-
Cracks on the surface	-	+	+/-	+/-
Cracks in the bedding	×	++	+	++
Pores on the surface	+/-	+	+	+
Pores in the bedding	×	++	+	++
Precipitated carbonates	×	+	+/-	+/-
Precipitated clays	×	+	++	+
Swelling clays	×	+	+	-
Banding textures	×	-	+	-

++ Present in a very large number and a predominant structure in the sample
\+ Present and also a dominant structure
+/- Present, but not as a dominant structure
\- Not present/found
× No data, so not able to say anything about this characteristic

6.2 Possible explanations

6.2.1 Dissolution and precipitation reactions

Changes in porosity and permeability due to mineral dissolution and precipitation can modify fluid flow *(Xu, Apps and Pruess, 2005)*, and is therefore an important feature to discuss. Dissolution and precipitation are two processes that are linked to each other. When a solid (formed by ionic bonds) reacts with water, the solid dissolves to form aqueous solutions, in which the solid dissociates into separate cations and anions. The process of dissolution continues until an equilibrium is reached between the solid and its component ions. When this equilibrium is disrupted (e.g. by addition of another common ion), it can occur that the solubility of the given solid changes. This would mean that the ions in solution are in excess compared to

the solid, and will want to reach equilibrium again by forming a precipitation. Precipitation is the process in which dissolved ions form a solid.

The three samples that have reacted with a fluid, all contain precipitation minerals, which automatically also means that dissolution has taken place. Clays are the most frequently seen precipitation minerals, with only minor carbonate precipitation. Mackenzie (2005) suggests possible reactions take place at a certain temperature range, in which common minerals in shales and sandstones dissolve and/or precipitate in contact with water. The most common minerals that cause dissolution and precipitation in shales, as described by Mackenzie (2005), are listed in table 4, along with the reaction formulas and the temperature at which dissolution or precipitation takes place.

Table 4. Possible dissolution and precipitation reactions of certain minerals found in shales. Adjusted from Mackenzie (2005) to fit the Gothic shale composition.

Material/mineral	Temperature (˚C)	Reaction
***Dissolution reactions: sources of dissolved components**		
Smectite	60–140	$K_{0.12}Na_{0.25}(Al_{1.41}Fe_{0.22}Mg_{0.41})(Si_{3.88}Al_{0.12})O_{10}(OH)_2 + 9.96H_2O = 0.12K^+ + 0.25Na^+ + 0.22\ Fe^{3+} + 0.41\ Mg^{2+} + 1.53Al^{3+} + 3.88H_4SiO_4 + 6.44OH^-$
Organic matter	40–100	$CH_2O + H_2O = CO_2 + 4H^+$
Kaolinite	75–150	$Al_2Si_2O_5(OH)_4 + 5H_2O = 2Al^{3+} + 2H_4SiO_4 + 6OH^-$
Calcite	>60	$CaCO_3 + 2H^+ = Ca^{2+} + CO_2 + H_2O$
***Precipitation reactions: sinks for dissolved components**		
Illite [a]	60–200	$0.65K^+ + 0.08Na^+ + 0.14Fe^{2+} + 0.2Mg^{2+} + 3.4H_4SiO_4 + 2.27Al^{3+} = K_{0.65}Na_{0.08}(Al_{1.68}Fe_{0.14}Mg_{0.2})(Si_{3.41}Al_{0.59})O_{10}(OH)_2 + 8.22H^+ + 2.69H_2O$
Chlorite [a]	60–200	$2.88Al^{3+} + 3.27Fe^{2+} + 0.96Mg^{2+} + 2.89H_4SiO_4 + 6.72H_2O = (Al_{1.77}Fe_{3.27}Mg_{0.96})Si_{2.89}Al_{1.11})O_{10}(OH)_8 + 17.1H^+$
Kaolinite/dicktite [b]	80–150	$2Al^{3+} + 2H_4SiO_4 + 6OH^- = Al_2Si_2O_5(OH)_4 + 5H_2O$
Calcite	100–160	$Ca^{2+} + CO_2 + H_2O = CaCO_3 + 2H^+$ (in the presence of active feldspar buffers)
	40–100	$Ca^{2+} + 2HCO_3^- = CaCO_3 + H_2O + CO_2$ (in the presence of organic alkanity)

a. Weathering reactions
b. In organic rich materials

The reactions listed in table 4 are probably the most common reactions that occur in the three reacted Gothic shale samples. This assumption is made due to the evidence found in the precipitated minerals. The precipitated minerals found in all three reacted samples were clay

and carbonate minerals, which is consistent with the precipitation reactions given in table 4. According to Kaszuba, Janecky and Snow (2005) the shale used in their study, which reacted with brine, did not contain any carbonate precipitation minerals. In this study it was observed that carbonates did precipitate in the brine reacted samples, due to the evidence for the formation of carbonates containing additional elements, observed using elemental compositions, which differ from the element distribution of the unreacted Gothic shale. These additional elements found in the precipitated carbonates in the reacted samples, were Fe and Mg. These carbonates are most likely be siderite or magnesite, which are not present in the unreacted Gothic shale (the starting material) according to both literature as well as this study. The dissolved Fe elements that are combined with carbonates could be originated from the pyrite minerals which dissolved in reaction with the brine or from dissolved clay minerals. The oxidation state of iron in pyrite is 2^+, and for siderite ($FeCO_3$) the oxidation state is also Fe^{2+}. This means that the oxidation state in the system of the shale does not change when the dissolved Fe elements of pyrite, precipitate into siderite. The dissolved Mg can only originate from dissolved clays.

6.2.2 Difference between surface and bedding planes

There is often a difference found between the surface of a sample and its corresponding bedding plane. Features such as cracks and pores are more dominant and present in the bedding planes, than they are at the surface of the sample. A reason for this phenomena is due to the natural weakness of the bedding planes compared to the surface of a shale.

As already stated in the introduction (chapter 1) the fissility is a characterization of a shale, which is a property that can cause thin layers to split easily along the closely spaced, parallel bedding planes. This is different for the surface of a shale as the fissility of the shale is only seen parallel to the bedding plane. The reason why shale has this characterization, is due to the orientation of the clay minerals, which are orientated parallel to the bedding plane.

Clays are generally agreed to be a primary causative factor that leads to shale instability *(Wilson and Wilson, 2014)*, although the exact mechanism involved is still debateable. Shale instability often causes serious operational problems for oil and gas exploration and production. Wilson and Wilson (2014) suggest two possible explanations for the link between clay mineralogy and shale instability:

1) It can be caused by the volume expansion of the clay minerals, following osmotic swelling and collapse of the interlayer space (see figure 3) of the clay.

2) Or it is caused by a mechanism which is related to the overlap of the double diffusive layer (see figure 4). This mechanism is associated with the charged external surfaces of the clay minerals exposed in opposing walls of micro- and mesopores of the shale, which then leads to a build-up of pore/hydration pressure *(Wilson and Wilson, 2014)*. This will then cause a contraction of the thickness of the double diffusive layer.

The cracks found in all the three samples are not only most prominent in the beddings planes, compared to the surface, but also often found to be parallel to the bedding planes (illustrated in figure 16). Keeping the above in mind, it is most likely due to the orientation of the clay minerals, and therefore the shale's fissility, what makes the bedding planes a weaker and therefore easier area for a fluid to react with.

For the oil and gas industry this is an important feature to know, as cracks are important contributors for the total porosity and permeability. The orientation of the shale can therefore play an important role when doing research about the shale gas site before actual drilling and fracking takes place, as estimations of the expected porosity can be calculated. But the orientation of the shale is probably not as important during the fracking process as it is during the experiments of this paper. The difference between these experiments and the technique of fracking, is that the samples discussed in this paper are put into a solution of the involved fluid, while fracking takes place under very high pressures. In these experiments, only the exterior of

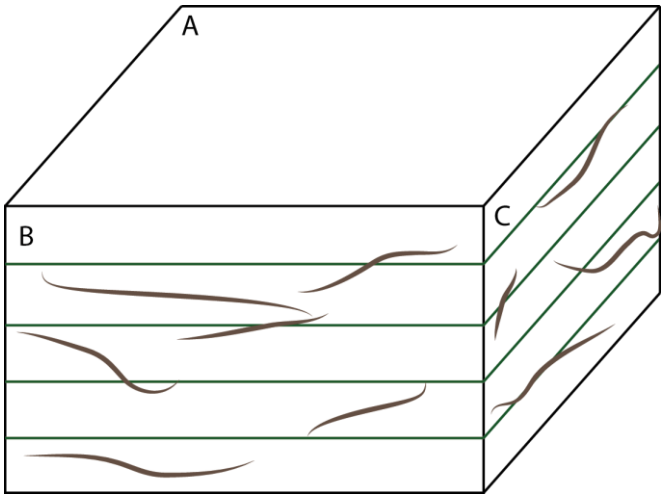

Figure 16. Schematic illustration of how the cracks are found in the reacted samples. The most cracks are found in the bedding planes of the sample (in B and C). These cracks in the bedding plane roughly follow the bedding plane orientation and are therefore more or less parallel to the bedding plane. In this figure no cracks are drawn on the surface of the sample (in A), but in the real samples there are a few cracks visible on the surface. The most cracks found on the surface of the sample, are found near the edges of the sample

the samples react with the fluid involved, in which the weaker places are the easier targets. When fracking, the pressure involved is so high that the shales break and form cracks in which the injected fluid can flow through (still under high pressure). The area that the fracking process reaches is much higher than that of the experiments done in this paper. This will therefore also cause a much larger amount of cracks to form, in both the bedding planes as well as on the surface. Nevertheless, fluid will always travel the furthest and easiest through natural weak spots of a material, in this case the bedding plane of the shale. Therefore the angle in which the shale should be drilled with respect to the bedding plane of the shale (i.e. the orientation of the clay minerals), might be relevant for the oil and gas industry as it might enhance the effectiveness of the fracking process. However this is not examined in detail in this study.

6.2.3 Banding textures

The banding textures found in the brine samples are hard to explain. The banding texture was not a consistent feature to be seen in all the brine samples, as only two out of the four brine reacted samples contained it. Nevertheless, all the other type of samples did not have the banding texture, making it a characteristic only seen in the brine reacted sample. This means that it can be assumed that the bands are most likely formed due to a reaction with the salt of the brine solution. The banding texture was only seen in the bedding planes of the samples and not at the surface.

Unfortunately the relief seen in the banding structures made it hard for the backscattered electron (BSE)-detector to detect and analyse the differences between the bands. When making an element map of the area with the banding texture, only the bands at a higher relief (with hardly/no pores) contained an element spectrum, while the bands with lower relief remained black (see figure 17).

The banding textures due to the reaction of brine with shale have not been explained or even mentioned once in a number of literature papers, making it harder to confirm possible reasons for this feature. It could simply be a feature which belongs to the bedding of the sample, but is now emphasized due to the relief differences. This relief difference could make it look as if there are big differences in porosity in the bedding, while it basically is only caused due to the differences in the roughness of the surface.

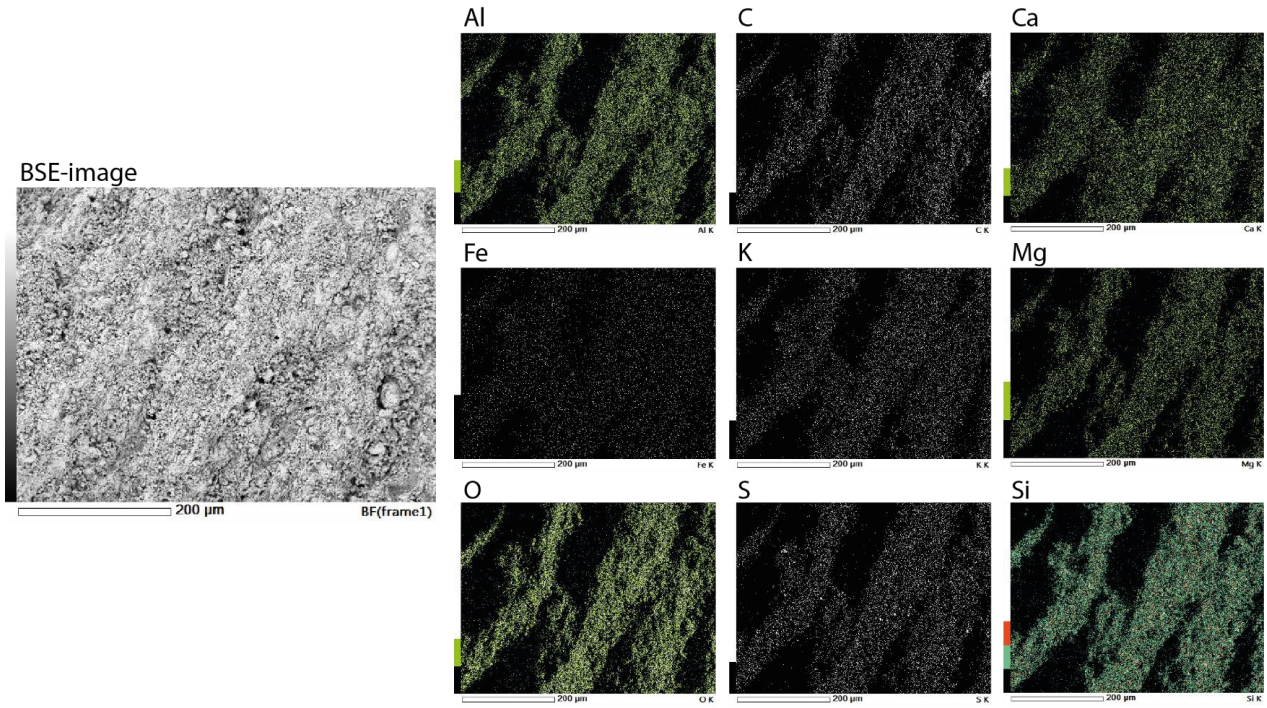

Figure 17. BSE-image made with the tabletop-SEM with corresponding element maps of the elements Al, C, Ca, Fe, K, Mg, O, S and Si. The dark (black) spots are not included in the element map due to the low relief and resemble the bands with a lot of pores. The bands that are included in the element mapping, are at a higher relief, and block the areas of low relief from the BSE-detector.

6.3 Theory overview

6.3.1 Swelling clays

As stated in the theory overview of chapter 3, several literature papers mentioned in that section expect that CO_2-fluid will not be a good fracking fluid due to the swelling of clays *(de Jong, Spiers and Busch, 2014; Giesting et al., 2012a; Giesting et al., 2012b; Busch et al., 2008).* These different authors have done research to find out if injecting CO_2-fluid into geological formation will cause clays in shales to swell and form a seal for the injected CO_2, storing the CO_2 in the subsurface. It appeared in their studies that CO_2-fluid is easily sorbed into clays and causes the clays to swell, decreasing the porosity and permeability in the shale rock. If this indeed would happen in every type of shale, CO_2-fluid would definitely not be a good fracking fluid.

However, the results gathered in this study do not necessarily agree with this. When looking at the unreacted sample and comparing it to the three fluid involved samples, the porosity has increased immensely, while the occurrence of swelling clays was only found in the brine and CO_2 samples. The amount of these swelling clays was very low in comparison with the amount of pores generated in the samples.

A possible reason for the findings of this study, is found in table 4. One of the dissolving minerals in a shale is likely to be smectite. Smectite, as already stated in chapter 3, is a swelling clay. Two of the possible precipitation minerals found in shales after dissolution takes place, are kaolinite and illite: two non-swelling clay minerals. It could be that after the unreacted Gothic shale has reacted with brine or CO_2-fluid, the amount of smectite has decreased due to dissolution, while the amount of illite/kaolinite increased. The swelling that takes place due to the involved fluid, is only seen in the left-over smectite minerals. This would explain why there is not much swelling found, but nonetheless still present.

6.3.2 Different type of shales

An important thing to keep in mind when doing research on shales, is that no shale is alike. While one type of shale might swell up intensely due to the reaction with the involved fluid, another type might have no swelling effects at all with the exact same fluid. This is because each shale has a different mineral content and therefore also a different content in its clay minerals. In the theory overview (chapter 3) and the previous section above, two types of clays have been mentioned: swelling and non-swelling clays. The percentages of these clays present in a shale, can depend the amount of swelling that occurs.

A factor which might also be important is the phenomena already discussed in the previous section. When a fluid reacts with a shale, dissolution and precipitation can take place, which can change the mineral content of the shale. The longer the fluid has time to react with the sample, the more likely equilibrium will be reached between the dissolution and precipitation phases. Hypothetical studies using the exact same shales can differ in outcome from each other due to the differences in reaction time used. While the first hypothetical study lets the sample sit in the fluid for 3 days, in which more dissolution takes place than precipitation, the second hypothetical study might have let the sample sit for 2 weeks, in which dissolution and precipitation reaches equilibrium. These two hypothetical studies will then most likely have different results in the amount of dissolution and precipitation phases.

6.3.3 CO_2 sequestration

Another question that arises when doing this study, is if CO_2 sequestration will actually work when using CO_2-fluid as a fracking fluid. There is still a lot of research done to evaluate and monitor CO_2 sequestration, as the process of geological sequestration has a lot of potential for geochemical reactions that are not yet fully understood *(Kaszuba, Janecky and Snow, 2003)*. Kaszuba, Janecky and Snow (2003) state that these reactions extend beyond simple aqueous

dissolution of CO_2 and precipitation of carbonate and may cause geochemical and geotechnical consequences for CO_2 sequestration.

When carbonates are formed due to the interaction of dissolved CO_2 with the shale, it can already be seen as a working CO_2 sequestration system. This is because mineral precipitation using aqueous CO_2 contents (forming carbonate precipitation) is one of the mechanisms of CO_2 retention (*Kaszuba, Janecky and Snow, 2003)*, along with stratigraphic and/or structural trapping and hydrodynamic trapping. But as stated in chapter 3, the reaction of CO_2-fluid with clays also plays an important role in CO_2 retention. When aqueous CO_2 reacts with clays, the CO_2-molecules have the tendency to be adsorbed by the clays, which in turn causes the clay to swell. The swelling of clays keeps the CO_2-molecules in place. Swelling clays were also observed in the carbonated Gothic shales samples. This feature is most likely also the reason why the amount of carbonate precipitation in the CO_2 reacted Gothic shales was less than would be expected of a sample that has reacted with CO_2.

6.4 Problems encountered

6.4.1 Different surfaces

There were a few problems encountered during this study. The biggest problem only came to light when most of the microscopic study was already conducted. The unreacted Gothic shale is the starting material for all the other samples. The only sample provided of the unreacted Gothic shale was imbedded in an epoxy and polished. The surface of the unreacted Gothic shale was therefore flat, instead of rough like the other samples. For this reason it is much harder to distinguish the changes of the other samples, compared to their starting material, as the surfaces are not the same. Due to the polished surface of the unreacted sample, a lot of the characteristics such as swelling clays were not able to be detected.

6.4.2 Over- and underestimation

A second problem encountered was during the analyzation of the images on their porosity in ImageJ. Thresholding the images to a grey scale in the program ImageJ, was needed to measure the porosity of a sample. As already mentioned in the methods section (chapter 4), during the process of thresholding the image, some very small pores may be overseen and therefore the total porosity might be underestimated. The other way around can happen as well during the thresholding-process, in which too many particles of the image are seen as pores, while they are actually not a pore. This will cause an overestimate of the pores. It can therefore

occur that one image is overestimated, while the other is underestimated, causing a much larger difference in the amount of pores between two measured samples than in reality.

6.4.3 Using an average

Another important thing to keep in mind on the analysis, is that even though the porosity seems to be spread out evenly across the surface and bedding planes for all samples, some images taken at a certain magnification can contain more or less pores relatively to the whole sample. Therefore it can occur that an image is used in this study, which may not be representative for the whole sample. In figure 18 this problem is illustrated in a simplified example; the top-left box shows the pores of the whole rock, which are approximately distributed evenly across the surface. The three smaller boxes A, B and C in the first box of figure 18, zoom in on this area. The zoomed in area A shows only two pores, while the zoomed in area B contains approximately 7.5 pores. For this example that is quite a difference, and both zoomed in areas are not representative for the whole, as the average amount of pores is between 4-5 ([pores A + pores B + pores C] / 3 = 4.5). Area C is therefore the most representative of the three zoomed in areas, with four pores. The best way to overcome this uncertainty is to take as much images of one sample at a certain magnification, and get an average of all the data measured (mean pore area surface, total pore area surface, standard deviation and number of pores). Providing an average is, in this study, better than providing the worst/best scenario, as it the most representative for the whole rock.

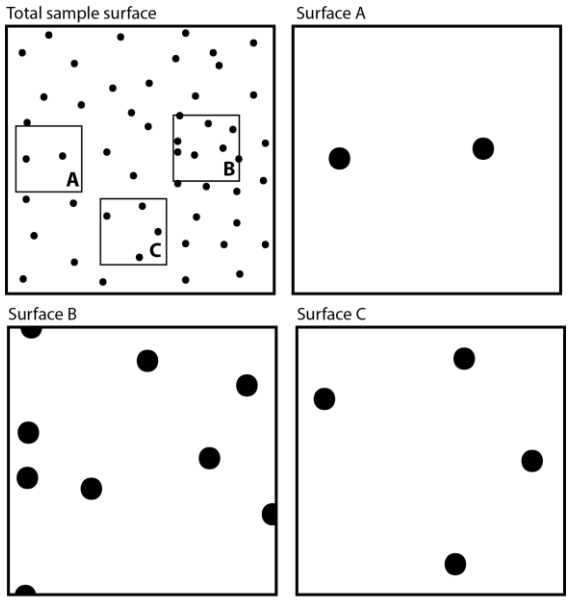

Figure 18. Simplified illustration showing how a SEM-image at a fixed magnification may not be representative for the whole rock. The top-left box shows the pores of the whole rock, which are approximately distributed evenly across the surface. The three smaller boxes A, B and C in the top-left box zoom in on this area. The zoomed in area A shows only two pores, while the zoomed in area B contains approximately 7.5 pores. For this example that is quite a difference, and both zoomed in areas are not representative for the whole, as the average amount of pores is between 4-5 ([pores A + pores B + pores C] / 3 = 4.5). Area C is therefore the most representative of the three zoomed in areas, with four pores.

7. CONCLUSION & FUTURE WORK

The work described in this thesis has been concerned with the possibility of a better and more environmental-friendly way to produce shale gas. The four different types of Gothic shale samples provided have been investigated at the nanoscale under the tabletop-SEM and FIB-SEM, with the aim to observe the changes in mineralogy and porosity between the four types of samples. In this final chapter the research question will be answered with the help of the research tasks established in the introduction (chapter 1.3), along with the implications for the oil/gas industry and will end with a few suggestions for future work on the scope of the thesis subject.

7.1 Conclusion

7.1.1 Research question and tasks

The research question of this thesis was *"Is CO_2-fluid suitable as an environment-friendly way of fracking and does it generate a higher porosity and permeability in shale gas sites, compared to the industrial ("normal") fracking fluid?"*. To answer the research question, the research tasks given in the introduction will have to be answered. The three research tasks formed in the introduction were the following:

1) How does the mineralogy of the shale rock change after reaction with fracking fluid, CO_2-fluid or brine?
2) Does the reaction with fracking fluid, CO_2-fluid or brine increase porosity in shales?
3) Do precipitated phases, e.g. clays, have a positive or negative impact on porosity generation in shale?

In short these questions will be answered in three bullets in respective order.

- In all three samples that have reacted with a fluid, no major mineralogy changes are found. The clay matrix stays the same and most of the carbonate minerals found in the unreacted Gothic shale, are still present in the other three samples. The alterations are seen in the precipitation minerals, where the precipitated clay minerals can be distinguished from the clay matrix, as the element distribution of the EDX-spectrum vary from each other.
- The porosity increases for all three samples that have interacted with the three different type of fluids. The sample that has reacted with brine shows the smallest increase in

porosity, and does not compete with the CO_2-fluid and industrial fracking fluid samples in the amount of pores generated. The CO_2-fluid and industrial fracking fluid have a much larger increase in porosity compared to both the unreacted Gothic shale sample as well as the brine reacted sample (see table 2) and compete with each other in the generation of porosity. There is no ultimate "winner" between these two samples (the fracking fluid and CO_2 reacted) in the amount of pores generated, as the amount of pores found in the two samples depend on the image and magnification used for measuring the porosity (as seen in table 2).

The 3D slab from the carbonated shale also showed insight in the way the CO_2-fluid infiltrated into the interior of the sample, instead of only reacting with the exterior of the sample. The 3D-slab revealed that cracks on the exterior are necessary to let a fluid infiltrate into the sample. When the fluid goes into the cracks, it reacts along the boundaries of the crack, creating pores in the interior of the sample, which would not have been formed if there were no cracks in the sample.

- The precipitated phases in the three fluids reacted Gothic shales definitely do not have an overall negative effect on the porosity generation in the shale, as the porosity increases significantly from the unreacted shale. But to say that it has a positive impact cannot be said either, as it might be that some of the precipitated phases have clogged certain pores that have been formed due to the dissolution reaction caused by the fluid involved. This suggests that if the precipitation phases did not occur, the porosity generation could probably have been much higher.

Now to finally answer the research question; it turns out that in this study, CO_2-fluid would be a good substitute for industrial fracking fluid for generating a higher porosity in shale gas sites. The amount of pores have increased significantly compared to the unreacted Gothic shale (see table 2). Not only does the amount of pores increase, but the sample reacted with CO_2-fluid also competes with the industrial fracking fluid sample in the amount of pores generated. Therefore it can be concluded that at the nanoscale experiments done in this thesis, CO_2-fluid would be a good fracking fluid for the Gothic shale sites, as it may also reduce the CO_2 emissions in the atmosphere. But unfortunately it is not that simple, as more research should be done to the connectivity of these pores to one another (=permeability). Without the pores being connected the gas flow into the induced fractures cannot be achieved. Each shale is different, and therefore reacts differently to fluids injected. The Gothic shale apparently contains minerals that do not cause a great deal of swelling when CO_2-fluid is injected into the shale nor does the precipitation

minerals cause clogging of the pores. Both the swelling and clogging could have a much larger effect when another type of shale comes in contact with CO_2-fluid. A solution for the swelling or non-swelling 'uncertainty' could be to inject a clay stabilizer, which is also a component in fracking fluid, along with the CO_2-fluid to prevent clays to swell when drilling for shale gas.

7.1.2 Implications for the oil/gas industry

To summarize what this means for the oil and gas industry, the findings which are relevant for the oil and gas industry will be highlighted in short:

- CO_2-fluid would work well as a fracking fluid as it generates the same amount, or even more, pores than the industrial fracking fluid.
- An even bigger increase in porosity could be possible if clay stabilizers are injected along with the CO_2-fluid to prevent clay swelling.
- Finding out the orientation of the clay layers, which are parallel to the bedding planes of the shale, might be useful when fracking. The orientation of the clay layers are most likely the reason why cracks form easier in the bedding planes of the shale than at the surface of the shale. The orientation of the shale can therefore play an important role when doing research about the shale gas site before actual drilling and fracking starts, as estimations of the expected porosity can be calculated (keeping the orientation of the clays in mind). The angle in which the shale should be drilled with respect to the bedding plane of the shale (i.e. the orientation of the clay minerals), might be relevant for the oil and gas industry as it might enhance the effectiveness of the fracking process. However this is not examined in detail in this study and should be examined in future work.

7.2 Future work

Although the results presented here have demonstrated that CO_2-fluid is an acceptable fracking fluid for the Gothic shale, it could be further developed in a number of ways:

- First of all it would be good to do more research to find out what happens in the interior of the samples and not only look at the exterior of the samples. This can be done with the FIB-SEM, which can cut into samples and produce an "inside-look" of the sample in the form of a 3D-slab of the sample. A beginning of this is done for the CO_2-fluid (EPA-1) sample, but because time and budget was running out, it was not continued for the other samples. This step is important for future work as it can provide information

about how deep the fluid can infiltrate into the shale, without the fracking process involved, and to find out if the permeability in the rock is connected to deeper parts of the samples, instead of staying at the surface.

- Another very important thing to keep in mind, is that no shale is alike. The Gothic shale reacts well with CO_2-fluid as the reaction between the two materials generates an increase in porosity compared to the unreacted Gothic shale, and competes with the industrial fracking fluid in the amount of pores generated. This, however, does not mean that every type of shale will have the same reaction with CO_2-fluid. The mineralogy of each shale is different and therefore a different type of shale might have the opposite effect as to what is observed in the Gothic shale. The CO_2-fluid could generate a decrease in porosity and cause clogging of pores due to the swelling of clays. The clay content of shale is therefore an important feature to know before drilling/fracking. This means that for each type of shale experiments such as in this thesis must be conducted, to find out how they react with the fluid involved, before it is used as a fracking fluid of shale gas.
- The observations and measurements of this study were conducted at the nanoscale and the samples themselves were only a few millimeters large. It would make a nice study to find out if the same observations and results are seen on bigger samples much larger than the samples used for this study. It would also make it easier to investigate the differences and compare the exterior of the samples to the interior of the samples.

ACKNOWLEDGEMENTS

I would like to thank dr. Helen E. King, dr. Oliver Plümper and dr. Paul R.D. Mason for providing me this subject for my master thesis. It helped a lot to work on an interesting and hot topic, which kept me motivated during the months working on my thesis. I would also like to thank both Helen King and Oliver Plümper for the help given in those past few months, when I got stuck on certain areas and for giving advice and things to think of during the writing process. I'd like to thank Oliver Plümper particularly for the introduction, help and time on the FIB-SEM. Also dr. Maartje Houben for helping me out with the sample preparation. Without the group of Dr. Kaszuba at the University of Wyoming, the samples would not have been produced and provided to Utrecht, so I would also like to thank them for providing the samples for this report and to make this study possible. And finally I would like to mention Miao Zhang, as he took the time to hand me some interesting literature on the topic of swelling clays due to CO_2-fluid.

REFERENCES

Anderson, R.L., Ratcliffe, I., Greenwell, H.C., Williams, P.A., Cliffe, S. and Coveney, P.V. (2010) *Clay swelling — A challenge in the oilfield*. Earth-Science Reviews, Volume 98, pp. 201–216

Barbeau, D.L. (2003) *A flexural model for the Paradox basin: Implications for the tectonics of the Ancestral Rocky Mountains*. Basin Research, Volume 15, pp. 97–115

Barteau, M. and Kota, S. (2014) *Shale Gas: A Game Changer for American Manufacturing*. Report of the "Shale gas symposium at National Press Club". University of Michigan Energy Institute

Boersma, T. and Johnson, C. (2012) *The Shale Gas Revolution: U.S. and EU Policy and Research Agendas*. Review of Policy Research, Volume 29, Issue Number 4, pp. 570–576

Broderick. J., Anderson, K., Wood, R., Gilbert, P., Sharmina, M., Footitt, A., Glynn, S. and Nicholls, F. (2011) *Shale gas: an updated assessment of environmental and climate change impacts.* A report commissioned by The Co-operative and undertaken by researchers at the Tyndall Centre, University of Manchester

Busch, A., Alles, S., Gensterblum, Y., Prinz, D., Dewhurst, D.N., Raven, M.D., Stanjek, H., and Krooss, B.M. (2008) *Carbon dioxide storage potential of shales*. International Journal of Greenhouse Gas Control, Volume 2, pp. 297–308

Busch, A., Alles, S., Krooss, B.M., Stanjek, H. and Dewhurst, D.N. (2009) *Effects of physical sorption and chemical reactions of CO2 in shaly caprocks*. Energy Procedia, Volume 1, pp. 3229–3235

Chalmers, G.R., Bustin, R.M. and Power, I.M. (2012) *Characterization of gas shale pore systems by porosimetry, pycnometry, surface area, and field emission scanning electron microscopy/transmission electron microscopy image analyses: Examples from the Barnett, Woodford, Haynesville, Marcellus, and Doig units*. The American Association of Petroleum Geologists Bulletin, Volume 96, Issue Number 6, pp. 1099–1119

Chen, B., Evans, J.R.G., Greenwell, H.C., Boulet, P., Coveney, P.V., Bowden, A.A. and Whiting, A. (2008) *A critical appraisal of polymer–clay nanocomposites.* Chemical Society Reviews, Volume 37, pp. 568–594

de Jong, S.M., Spiers, C.J. and Busch, A. (2014) *Development of swelling strain in smectite clays through exposure to carbon dioxide*. International Journal of Greenhouse Gas Control, Volume 24, pp. 149–161

Elliot, T.R. and Celia, M.A. (2012) *Potential Restrictions for CO_2 Sequestration Sites due to Shale and Tight Gas Production.* Environmental Science & Technology, Volume 46, Issue Number 7, pp. 4223–4227

Environmental Protection Agency (2012) *Study of the Potential Impacts of Hydraulic Fracturing on Drinking Water Resources: Progress report*. EPA Publication: EPA/601/R-12/011. Office of Research and Development, Washington D.C.: U.S. Environmental Protection Agency

European Commission (2014) Commission Staff Working Document Impact Assessment, accompanying the Communication from the Commission on the *exploration and production of hydrocarbons (such as shale gas) using high volume hydraulic fracturing in the EU*. Bureau of pubications of The European Commission. 23 final, part ¼

Ferrer, I. and Thurman, E.M. (2015) *Chemical constituents and analytical approaches for hydraulic fracturing waters.* Trends in Environmental Analytical Chemistry, Volume 5, pp. 18–25

Giesting, P., Guggenheim, S., Koster van Groos, A.F. and Busch, A. (2012a) *Interaction of carbon dioxide with Na-exchanged montmorillonite at pressures to 640 bars: Implications for CO2 sequestration*. International Journal of Greenhouse Gas Control, Volume 8, pp.73–81

Giesting, P., Guggenheim, S., Koster van Groos, A.F. and Busch, A. (2012b) *X-ray Diffraction Study of K- and Ca-Exchanged Montmorillonites inCO2 Atmospheres*. Environmental Science and Technology, Volume 46, Issue Number 10, pp. 5623−5630

Goldhammer, R.K., Oswald, E.J. and Dunn, P.A. (1991) *Hierarchy of stratigraphic forcing: Example from Middle Pennsylvanian shelf carbonates of the Paradox basin*. Kansas Geological Survey, Bulletin 233, pp. 361–413

Goldhammer, R.K., Oswald, E.J. and Dunn, P.A. (1994) *High-frequency, glacio-eustatic cyclicity in the Middle Pennsylvanian of the Paradox Basin: an evaluation of Milankovitch forcing.* Special Publications of the International Associations of Sedimentologists, Volume 19, pp. 243–283

Grim, R.E. (1968) *Clay Mineralogy, 2nd Edition.* McGraw-Hill Book Company, New York.

Guo, C., Xu, J., Wu, K., Wei, M. And Liu, S. (2015) *Study on gas flow through nano pores of shale gas reservoirs*. Fuel, Volume 143, pp. 107–117

Hanshaw, B.B. and Hill, G.A. (1969) *Geochemistry and Hydrodynamics of the Paradox Basin Region, Utah, Colorado and New Mexico.* Chemical Geology, Volume 4, pp. 263–294

Heath, J.E, Dewers, T.A., McPherson, B.J.O.L., Petrusak, R., Chidsey Jr., T.C., Rinehart, A.J. and Mozley, P.S. (2011) *Pore networks in continental and marine mudstones: Characteristics and controls on sealing behavior*. Geosphere, Volume 7, Issue Number 2, pp. 429–454

Hensen, E.J.M. and Smit, B. (2002) *Why Clays Swell.* Journal of Physical Chemistry B, Volume 106, Issue Number 49, pp. 12664–12667

Howarth, R.W., Ingraffea, A. and Engelder, T. (2011) *Natural gas: Should fracking stop?* Nature, Volume 477, pp. 271–275

Howarth, R.W., Santoro, R. and Ingraffea, A. (2011) *Methane and the greenhouse-gas footprint of natural gas from shale formations*. Climatic Change, Volume 106, pp. 679–690

International Energy Agency (2011) *Are we entering a golden age of gas*; World Energy Outlook 2011, Special Report; http://www.iea.org/weo/docs/weo2011/WEO2011_GoldenAgeofGasReport.pdf.

Jacoby, H.D., O'Sullivan, F.M. and Paltsev, S. (2011) *The Influence of Shale gas on U.S. Energy and Environmental Policy.* Economics of Energy & Environmental Policy, 2012, Volume 1, Issue Number 1, pp. 37–51

Jung, H.B., Um, W. and Cantrell, K.J. (2013) *Effect of oxygen co-injected with carbon dioxide on Gothic shale caprock–CO2–brine interaction during geologic carbon sequestration*. Chemical Geology 354, pp. 1–14

Kang, S.M., Fathi, E., Ambrose, R.J., Akkutlu, I.Y. and Sigal, R.F. (2011) *Carbon dioxide storage capacity of organic-rich shale*. Society of Petroleum Engineers Journal, SPE 134583

Kaszuba, J.P., Janecky, D.R. and Snow, M.G. (2003) *Carbon dioxide reaction processes in a model brine aquifer at 200 ˚C and 200 bars: implications for geologic sequestration of carbon*. Applied Geochemistry, Volume 217, pp. 277–293

Kaszuba, J.P., Janecky, D.R. and Snow, M.G. (2005) *Experimental evaluation of mixed fluid reactions between supercritical carbon dioxide and NaCl brine: Relevance to the integrity of a geologic carbon repository*. Chemical Geology, Volume 18, pp. 1065–1080

Lawton, T.F. and Buck, B.J. (2006) *Implications of diapir-derived detritus and gypsic paleosols in Lower Triassic strata near the Castle Valley salt wall, Paradox Basin, Utah*. Geology, Volume 34, Issue Number 10, pp. 885–888

Lewis, A.M. and Hughes, R.G. (2008) *Production Data Analysis of Shale Gas Reservoirs.* Society of Petroleum Engineers. doi:10.2118/116688-MS

Madsen, F.T. and Müller-Vonmoos, M. (1989) *The Swelling Behaviour of Clays*. Applied Clay Science, Volume 4, pp. 143–156

Marcon, V. and Kaszuba, J.P. (2015) *Carbon dioxide-brine-rock interactions in a carbonate reservoir capped by shale: Experimental insights regarding the evolution of trace metals.* Paper still in review for publishment.

Mohajan, H.K. (2012) *Unconventional Shale Gas Extraction: Present and Future Affects*. International Journal of Human Development and Sustainability, Volume 5, Issue Number 2, pp. 9–23

Nicot, J-P. and Duncan, I.J. (2012) *Common attributes of hydraulically fractured oil and gas production and CO2 geological sequestration*. Greenhouse Gas Science Technology, Volume 2, pp. 352–368

Pacheco, K.W. (2013) *Petroleum potential for the Gothic Shale, Paradox Formation in the Ute Mountain Ute Reservation, Colorado and New Mexico.* MSc Thesis. Colorado School of Mines: USA

Pinnavaia, T.J. (1983) *Intercalated clay catalysts*. Science, Volume 220, pp. 365–371.

Preibisch, S., Saalfeld, S. and Tomancak, P. (2009) *Globally optimal stitching of tiled 3D microscopic image acquisitions*. Bioinformatics, Volume 25, Issue Number 11, pp. 1463-1465

Rahm, B.G., Riha, S.J. (2012) *Toward strategic management of shale gas development:Regional, collective impacts on water resources*. Environmental Science & Policy, Volume 17, pp. 12–23 doi:10.1016/j. envsci.2011.12.004

Rasband, W.S. (2014) *ImageJ*. U. S. National Institutes of Health, Bethesda, Maryland, USA, http://imagej.nih.gov/ij/, 1997-2014

Schädlich, B., Marcher, T. and Schweiger, H.F. (2012) *Application of a constitutive model for swelling rock to tunneling*. Geotechnical Engineering Journal of the SEAGS & AGSSEA, Volume 43, Issue Number 4, pp. 47-53

Slingerland, S., Rothengatter, N., van der Veen, R., Bolscher, H. And Rademakers, K. (2014) *Economic Impacts of Shale Gas in the Netherlands*. Triple E Consulting – Energy, Environment & Economics B.V., Rotterdam, the Netherlands. TEC1048NL

SRU, German Advisory Council of the Environment (2013) *Fracking for Shale Gas Production: A contribution to its appraisal in the context of energy and environment policy*. Statement no. 18

Stephenson, T., Valle, J.E. and Riviera-Palou, X. (2011) *Modeling the Relative GHG Emissions of Conventional and Shale Gas Production*. Environmental Science & Technology, Volume 45, Issue Number 24, pp. 10757–10764

Stevenson, G.M. and Baars, D.L. (1986) *The Paradox; a pull-apart basin of Pennsylvanian age.* Paleotectionics and Sedimentation in the Rocky Mountains Region, United States, Volume 41, pp. 513–539

Trudgill, B.D. (2011) *Evolution of salt structures in the northern Paradox Basin: controls on evaporite deposition, salt wall growth and supra-salt stratigraphic architecture.* Basin Research 23, pp. 208–238

Vetter, A. (2015) *Shale gas in Germany – the current status*. GFZ German Research Centre for Geosciences

Vidic, R.D., Brantley, S.L., Vandenbossche, J.M., Yoxtheimer, D. and Abad, J.D. (2013) *Impact of Shale Gas Development on Regional Water Quality*. Science, Volume 340, Issue Number 6134, 1235009

Vos, A. (2014) *Shale gas extraction: In line with the general (environmental) principles of Union and Dutch law?* MSc Thesis. Utrecht University, the Netherlands

Wang, Y. (2014) *Nanogeochemistry: Nanostructures, emergent properties and their control on geochemical reactions and mass transfers*. Chemical Geology 378-379, pp. 1–23

White, E., Fell, M., Smith, L. and Keep, M. (2015) *Shale gas and fracking*. Science and Environment Section & Social and General Statistics Section. Parliament UK, Commons Briefing papers SN06073

Wilson, M.J. and Wilson, L. (2014) *Clay mineralogy and shale instability: an alternative conceptual analysis*. Clay Minerals, Volume 49, pp. 127–145

Xu, T., Apps, J.A. and Pruess, K. (2005) *Mineral sequestration of carbon dioxide in a sandstone–shale system*. Chemical Geology, Volume 217, Issue Numbers 3–4, pp. 295–318

Ziarani, A.S. and Aguilera, R. (2012) *Knudsen's Permeability Correction for Tight Porous Media*. Transp Porous Med, Volume 91, pp. 239–260